CLW-4-5085

8-7-80

DRAFT

GRAIN BOUNDARY SEGREGATION AND INTERGRANULAR FAILURE*

CONF-800519--1 (Draft)

C. L. White
Metals and Ceramics Division
Oak Ridge National Laboratory
Oak Ridge, Tennessee 37830

ABSTRACT

Trace elements and impurities often segregate strongly to grain boundaries in metals and alloys. Concentrations of these elements at grain boundaries are often 10^3 to 10^5 times as great as their overall concentration in the alloy. Because of such segregation, certain trace elements can exert a disproportionate influence on material properties. One frequently observed consequence of trace element segregation to grain boundaries is the occurrence of grain boundary failure and low ductility. Less well known are incidences of improved ductility and inhibition of grain boundary fracture resulting from trace element segregation to grain boundaries in certain systems.

An overview of trace element segregation and intergranular failure in a variety of alloy systems as well as preliminary results from studies on Al–3% Li will be presented.

MASTER

*Research sponsored by the Division of Materials Sciences, U.S. Department of Energy, under contract W-7405-eng-26 with the Union Carbide Corporation, and contract EY-76-C-05-033 with Oak Ridge Associated Universities.

INTRODUCTION

Trace elements and impurities can sometimes concentrate at grain boundaries and other interfaces in polycrystalline alloys. Such solute enriched regions (often only 2-3 atom layers thick) may be 10^3 to 10^5 times richer in solute than the rest-of-the-grains. The existence of such solute rich regions, forming a continuous network throughout the alloy, can have profound effects on its metallurgical properties.

One frequently observed result of segregation* is the occurrance of brittle, intergranular failure. Significant losses in strength as well as ductility are often associated with segregation. Because these effects result from extremely low overall concentrations of impurities (often less than 100 ppm), the identity of the segregating and embrittling species often escapes detection by conventional trace element analysis. The recent availability of several powerful analytical techniques has permitted direct identification of segregating elements in many cases. Information of this kind is, in turn, contributing to a fundamental understanding of how segregation induced fracture occurs.

The purpose of this paper is to review the current understanding of segregation, and its role in intergranular failure. An overview of the existing

*For the sake of brevity, the term "segregation" will be understood to mean "solute segregation to grain boundaries."

experimental observations, as well as theoretical models, will be presented. In several instances, conflicting models and interpretation have received attention, and so far as possible, the significance of these differences will be discussed. For the sake of simplicity and brevity, only the effects of equilibrium segregation in single phase binary alloys will be addressed. Experimental observations on multiphase and multicomponent systems will be referenced, however, if the precipitation and extra components are not considered to strongly influence the observation.

Grain Boundary Fracture

Grain boundary fracture involves the nucleation and propagation of nearly brittle cracks along grain boundaries. These cracks are described as "nearly brittle" because while they are often free from any signs of ductile tearing or dimpling, significant bulk deformation can occur prior to failure, and evidence of slip processes can often be observed on fracture surfaces (see Figs. 1 and 2).

Grain boundary fracture is most often associated with trace element segregation to grain boundaries. Table I lists a representative, although not exhaustive, list of alloy-trace element combinations where segregation and embrittlement are known to occur. One striking feature of this table is the consistency with which metalloid elements (P, S, Se, Sn, Sb, Te, Bi, and Pb) segregate to, and embrittle, grain boundaries. The tendency of these elements to segregate strongly to surfaces in molten alloys is well known, and in most cases, this general class of elements also appears to segregate strongly to free surfaces and interphase boundaries in polycrystalline alloys.

In spite of the overwhelming empirical correlation between trace impurity segregation and intergranular fracture, there has never been a satisfactory explanation of why these metalloid impurities have such a propensity for inducing intergranular fracture. Indeed the more fundamental question of why all polycrystalline metals, even those that are very pure, do not fail intergranularly has never been fully explained. It seems that the disruption of atomic structure associated with the grain boundary would provide a preferred path for fracture, especially in metals that cleave transgranularly (and whose bulk deformation properties are therefore capable of allowing a sharp crack to propagate without extensive blunting).

Because of the long historical connection between grain boundary fracture and trace impurity segregation, it had been assumed until recently that: (1) all grain boundary fracture is the result of trace impurity segregation (i.e., clean grain boundaries will not fail) and (2) any trace element segregation to grain boundaries is detrimental. These assumptions seemed to be supported by the general observation that most metals, if sufficiently pure, do not fail intergranularly, and that surface analysis of intergranular fracture surfaces nearly always revealed segregated impurities.

Both of the above "rules" have recently been confronted with exceptions. Iridium (51), Pt + 30% Rh + 8% W (52), and Fe + 12% Mn (53) have all been shown to fail intergranularly, apparently without being embrittled by trace impurities.* Conversely the ductility of these alloys can be significantly improved by ppm level additions of thorium (for iridium) or boron (for Pt + 30% Rh + 8% W and Fe + 12% Mn). In all three cases, the trace element addition responsible for ductilizing the alloy segregates strongly to the grain boundaries.

Given the many years that segregation-induced embrittlement has endured without a truly satisfactory explanation, it is not surprising that the kind of ductilizing effects noted above have not been explained either. Noting that the ductilizing effects of segregation have only been observed in alloys that have intrinsically weak boundaries to begin with, one might be tempted to suggest that, in these particular alloys, any segregation might result in some improvement. This argument is belied by the fact that other segregating and embrittling impurities are known for both Ir + 0.3 W [embrittled by phosphorus (50)] and Pt + 30% Rh + 8% W

*Unless otherwise stated, all compositions reported in this paper are percent, or parts per million (ppm) by weight.

[embrittled by Se (48)]. While there is no evidence to support the contention, it seems likely that one or more of the metalloids will segregate in, and embrittle, Fe + 12 Mn.

Given the fact that segregation of trace impurities to grain boundaries occurs and is often associated with dramatic changes (either increases or decreases) in ductility, the central question is "by what mechanism do these effects occur?" What makes one element beneficial and another detrimental? The following sections of this paper address the major considerations associated with grain boundary fracture; however, a detailed mechanistic understanding has yet to be achieved.

Grain Boundary Segregation

Figure 3 is a schematic representation of a 38° 100 tilt boundary in an fcc crystal having an equilibrium spacing, δ_{AA}, between solute atoms in the perfect lattice. Two segments of this repeating structure are shown, with ten different "grain boundary atoms" identified. Some of the grain boundary atoms do not lie on lattice sites of either adjacent crystal, but have been relaxed to take up intermediate positions. This relaxation

process, which minimizes the energy of the boundary subject to the constraints of the adjacent lattices, results in stretching (e.g., $\delta_{19} > \delta_{AA}$) or compression ($\delta_{45} < \delta_{AA}$) of interatomic bonds at the boundary. This, in turn, results in net attractions and repulsions between various pairs of atoms according to the sign of their displacement from equilibrium. Obviously, mechanical equilibrium requires that the net force across any macroscopic region of boundary to be zero.

The energetics of solute segregation can be visualized by considering the hypothetical interatomic potentials between solvent (A) and solute (B) atoms shown in Fig. 4 along with the structure indicated in Fig. 3. Curve "a" in Fig. 4 shows the interaction between two A atoms. Their equilibrium spacing is δ_{AA} and the energy required to separate them to infinite distance is ε_{AA}. Curve "b" shows the interaction between neighboring A and B atoms, where ε_{AB} is their equilibrium binding energy, and δ_{AB}, their equilibrium spacing.*

When a B atom resides in the bulk lattice, it is constrained by the surrounding lattice of A atoms to maintain an interatomic spacing nearly

*For sake of simplicity, solute-solute (B-B) interactions will be neglected.

equal to δ_{AA}. This results in an effective binding energy ε'_{AB}, which is smaller in magnitude than ε_{AB}. If a B atom could find a location where neighboring A atoms are more nearly a distance δ_{AB} away, then its contribution to the energy of the system would be decreased. Likewise, an A atom at a grain boundary (e.g., at site #1 in Fig. 3) can be displaced from its equilibrium lattice site on either adjacent grain, resulting in a lower binding energy, ε'_{AA}, than for A atoms in the perfect lattice. Clearly, an appropriate exchange between B atoms in the lattice and A atoms in the boundary can result in a significant decrease in the overall energy inventory of the system.

A rigid exchange between a B atom in a lattice site, and an A atom at site #1 in Fig. 4, would constitute such an appropriate excharge. The net energy change for bond 1-9, which we will call $\Delta\varepsilon_{19}$, is equal to $(\varepsilon_{AB} - \varepsilon'_{AB}) + (\varepsilon_{AA} - \varepsilon'_{AA})$. Because there are other stretched bonds around site #1, the total energy change associated with this rigid exchange may be significantly larger than the value of $\Delta\varepsilon_{19}$. Finally, if the grain boundary structu is allowed to relax following the rigid exchange, the energy of the system will be lowered even further. Such relaxations are necessary in order to

assure that the net force on a given atom or group of atoms is zero. The total energy change, $\Delta\varepsilon_{B1}$, associated with a fully relaxed (equilibrium) transfer of a B atom to site #1 will be called the "interaction energy" between a B atom and site #1.

A statistical thermodynamic treatment of segregation based on solid-state analog of Langmuir adsorption in gas-metal systems (1) was developed by McLean (54). This treatment assumes that all grain boundary sites have either a single valued interaction energy, $\Delta\varepsilon$, with a particular solute, or they have no interaction at all. These assumptions permit an expression to be developed relating the fraction of these energetically attractive grain boundary sites that are occupied by solute atoms, X_B^b, the fraction of solute atoms in the lattice, X_B^ℓ, and the absolute temperature at which equilibration takes place, T, [see Eq. (1)].*

$$X_B^b = \frac{X_B^\ell \exp(\frac{\Delta\varepsilon}{kT})}{1 - X_B^\ell + X_B^\ell \exp(\frac{\Delta\varepsilon}{kT})} \qquad (1)$$

McLean suggested that approximately one third of the "grain boundary" sites might have an attractive interaction with solute atoms. If the boundary is then assumed to be on the order of three atom layers thick, the areal density of energetically favorable sites is one monolayer.† Equation (1) predicts that X_B^b

*Throughout this paper subscripts A and B will denote solvent and solute species, respectively. Lower case subscripts, or superscripts (e.g., b, ℓ, s) will denote the microstructural feature (e.g., boundary, lattice, surface) to which a variable pertains.

†The average areal density of atoms (i.e., an average monolayer) in nickel is approximately 2×10^{19} atom/m^2.

will decrease as T is increased, and have a roughly linear dependence of X_B^b on X_B^2 for small values of X_B^b. These qualitative predictions are in general agreement with experimental observation, however, some discrepancies in detail do exist. Several studies of segregation over a range of temperatures indicate that the temperature dependence of X_B^b is not as strong as is predicted by Eq. (1) (47,55). This behavior can be explained by lifting the assumption that all segregating atoms have the same interaction energy, $\Delta\varepsilon$. Seah and Hondros (55) have modified a gas-solid adsorption model first suggested by Branauer, et al. (63,64) and White and Stein (47) have suggested a "spectrum of binding energies" approach, both of which allow the effective interaction energy between segregating solute atoms and grain boundary sites to vary according to fraction of sites already occupied.

An alternate approach to segregation, based on the classical interfacial thermodynamics of Gibbs (56,57,58) addresses the relationship between segregation and interfacial energetics. In the Gibbs' approach, the extent of segregation is defined by the solute "adsorption," Γ_B, of component B at an interface. Figure 5-a shows concentration profiles across a grain boundary in a hypothetical binary (A-B) system. The grain boundary solute adsorption, Γ_B^b, equals the shaded area under the C_B versus z curve in Fig. 5-a. For binary systems, it is convenient to define $\Gamma_{B(A)}^b$, the

"relative adsorption of B with respect to A" (61) as in Eq. (2).

$$\Gamma^{b}_{B(A)} = \Gamma^{b}_{B} - \left(\frac{X_B}{1 - X_B}\right) \Gamma^{b}_{A} \qquad (2\ )$$

where

X_B = atom fraction of B in the bulk lattice.

For systems where segregation of B is large, and X_B is small, $\Gamma_{B(A)} \simeq \Gamma_B$.

The Gibbs adsorption equation for a grain boundary in a binary system relates equilibrium changes in grain boundary energy to changes in chemical potential and temperature:

$$d\gamma_b = s_b dT - \Gamma^{b}_{B(A)}\, d\mu_B \qquad (3)$$

where γ_b is the specific grain boundary energy, s_b is the specific grain boundary entropy,* and μ_B is the chemical potential of component B.

---

*In general, s_b will reflect contributions from both vibrational effects (e.g., stretched and broken bonds), and configurational effects.

For an isothermal system, where the component B has segregated to the grain boundary (i.e., $\Gamma^{b}_{B(A)} > 0$), an infinitesimal increase in μ_B will produce an infinitesimal decrease in γ_b. The physical basis for this effect involves the relaxation of distorted interatomic bonds as discussed at the beginning of this section.

Similar equations can be written to describe solute adsorption at free surfaces. In general, specific interfacial energies are expected to decrease as a result of equilibrium segregation. This effect will be discussed further with regard to the energetics of brittle crack propagation.

Up to this point we have largely ignored the chemical nature of segregating solutes. The body of available experimental information suggests several general characteristics of solvent-solute systems where significant segregation occurs. McLean has noted that misfitting solute atoms (over- or under-size) might find energetically more favorable sites at grain boundaries than in the bulk lattice (54). The concept of size misfit was extended by

White and Coghlan (59) to include modulus interactions. Such interactions can occur in the absence of any size misfit, so long as there is distortion associated with the grain boundary structure. Similar effects have been reported by Machlin and Levi (67) in lattice modeling studies of segregation, using empirical interatomic potentials. Seah and Hondros (55) noted an inverse relationship between grain boundary enrichment of a solute, and its solubility in the solvent lattice. All of the above factors (size, modulus, solubility) reflect the chemical interaction of solute and solvent species.

One class of solute-solvent pairs which seems to exhibit consistently extensive segregation are metalloid elements (S, P, Sb, As, Sn) in transition metals (Fe, Ni) (33). The surface activity of metalloid elements in molten transition metals is well known (35), and their tendency to segregate strongly and reduce interfacial tensions in the solid state is also becoming well established (36). While these are not the only solute-solvent pairs known to exhibit segregation, they do seem to be associated consistently with grain boundary fracture.

Effects of Segregation on Grain Boundary Fracture

Discussions of segregation induced intergranular fracture have, to a very large extent, centered around the effects of segregation on the cohesive energy, ϕ_c, and the cohesive stress, σ_c, of the grain boundary. Recently, the effects of segregation on the nature of interatomic bonding and crack tip plasticity have also been addressed. These factors are discussed in this section.

Cohesive Energy: The cohesive energy of a grain boundary, ϕ_c, is defined as the energy required to separate reversibly the two adjacent grains to form free surfaces. Because this process involves destruction of grain boundary area and creation of free surface area, ϕ_c can be expressed in terms of the specific grain boundary and surface energies (2–5):

$$\phi_c = 2\gamma_s - \gamma_b \qquad (4)$$

It is through the dependence of γ_s and γ_b on $\Gamma^s_{B(A)}$ and $\Gamma^b_{B(A)}$ (the surface and grain boundary adsorption of impurities) indicated by Eq. (3) that solute segregation can affect ϕ_c.

Hondros (1) has measured γ_s and γ_b for Fe-P alloys at 1450 C (see Fig. 6-a). As expected for a solute that is known to segregate to both grain boundaries (37) and free surfaces (36), phosphorus is observed to lower γ_s and γ_b. Given the data in Fig. 6-a, and assuming Henrian behavior (65) of phosphorus in Fe, Hondros rearranged Eq. (3) to express Γ_P as:

$$\Gamma_P = - \frac{1}{2.303\ RT} \left(\frac{\partial \gamma}{\partial \log_{10} X_P} \right) \qquad (5)$$

He then plotted the resulting values of Γ_P^s and Γ_P^b as a function of X_P^ℓ, as shown in Fig. 6-b.

Several authors (2–5) have noted that during brittle intergranular fracture at low temperatures, crack propagation generally occurs so rapidly that the newly created free surfaces will not be in equilibrium with the bulk composition of the adjacent grains. These newly created surfaces will "inherit" one-half of the excess solute segregated to the grain boundary as shown in Fig. 5-b. Except for the special case where the equilibrium value of $\Gamma^s_{B(A)} = 1/2\ \Gamma^b_{B(A)}$, the specific free energy of this rapidly created free surface, γ_s^*, will not equal the equilibrium value, γ_s. This consideration results in a modified form of Eq. (4), to describe the energy, ϕ_c^*, required to reversibly separate adjacent grains subject to the constraint that $\Gamma^s_{B(A)}$ for each resulting surface equals $\Gamma^b_{B(A)}/2$.

$$\phi_c^* = 2\gamma_s^* - \gamma_b \qquad (5)$$

Evaluation of γ_s^*, and subsequently ϕ_s^*, from data such as that in Fig. 6, has been the subject of several recent theoretical studies. Seah (3) has argued that γ_s^* should depend primarily on $\Gamma^s_{B(A)}$, and not on bulk concentration, X_B^{ℓ}. He considered that the surface energy, γ_s^H, of a hypothetical alloy (see Fig. 5-d) having an impurity concentration, C_B^H, such that the corresponding equilibrium surface adsorption $\Gamma^{sH}_{B(A)}$ equals $\Gamma^b_{B(A)}/2$. Seah argued that γ_s^H approximately equals γ_s^* since both surfaces have the same level of adsorption.

For a bulk phosphorus concentration of 0.0316 at % in iron ($\log X_P^{\ell} = -1.5$), Hondros' data in Fig. 6.b (dotted line) indicates $\Gamma_P^b \simeq 2.2 \times 10^{-10}$ mole/cm^2, yielding $\Gamma_P^{sH} = 1.1 \times 10^{-10}$ mole/cm^2, and $X_P^H \simeq 0.00615$ at % ($\log_{10} X_P^H = -2.211$ (see dashed line in Fig. 6-b)). The surface energy of this hypothetical alloy γ_s^H, then is 2060 erg/cm^2 (dashed line in Fig. 6-a), yielding $\phi_c^* = [2\gamma_s^H - \gamma_b] = [2(2060)-760]$ erg/cm^2. Similarly calculated values for $X_P = 0.100$ and 0.316 at. % are given in Table IV and plotted in Fig. 7. Clearly, to the extent that Seah's argument is correct, the effect of X_P on ϕ_c^* in iron at 1450 C is small. Based on a detailed study of adsorption isotherms for trace element segregation to both surfaces and grain boundaries, Seah concluded that solute segregation will generally have little effect on ϕ_c^*.

Seah's approach to estimating ϕ_c^* has been criticised by a number of investigators (24,4,5). Hirth (4) and Hirth and Rice (5) have examined Seah's assumption

$\phi_c^* = 2\,\gamma_s^H - \gamma_b$, and concluded that it neglects a term they call the "work of adsorption." They derive an expression equivalent to Eq. (6) to describe ϕ_c^*.

$$\phi_c^* = 2\,\gamma_s^H - \gamma_b - \Gamma_{B(A)}^b\,(\mu_B - \mu_B^H) \qquad (6)$$

where:

μ_B = the chemical potential of component B in alloy

μ_B^H = The chemical potential of component B in the hypothetical alloy.

For solute-solvent systems where segregation occurs more strongly to free surfaces than to grain boundaries, μ_B^H will be less than μ_B, and the correction term, $\Gamma_{B(A)}^b[\mu_B - \mu_B^H]$, will be positive. The data in Figs. 6-a and 6-b indicate that this is the case for P in Fe at 1450 C, and values of ϕ_c^* calculated according to Eq. (6) are reported in Table II. These values are also plotted as a function of X_P^ℓ in Fig. 7 and are in good agreement with similar, but more extensive, calculations by Asaro (2).

The correction term, $\Gamma_{B(A)}^b([\mu_B - \mu_B^H])$, introduced by Hirth and Rice accounts for the change in chemical potential of the adsorbed grain boundary atoms as they are transferred from a grain boundary environment (μ_B) to a free surface environment (μ_B^H). This correction assumes the free surface is independent of the bulk, and free to relax locally, but not to exchange atoms with the bulk in a diffusive manner.

only a
Unfortunately, there are/few solute-solvent systems for which the type of data in Fig. 6 are available. It seems likely, however, that effects of segregating metalloid solutes on ϕ_c^*, of the magnitude shown in Fig. 7 (i.e., 10–20% decreases) according to the Hirth-Rice formula are a fairly general phenomenon.

Cohesive Stress: The cohesive stress, σ_c, of a grain boundary is the maximum force per unit area required to uniformly separate two adjacent grains along their common boundary. Figure 8-a shows a hypothetical plot of energy (ϕ) versus separation (δ) for a uniformly separating, planar grain boundary. Figure 8-b shows the corresponding plot of stress (σ) versus separation, where $\sigma(\delta) = \partial\phi/\partial\delta$. Grain boundaries are not observed to separate uniformly, however, so σ_c cannot be directly measured. Orowan (15) obtained a rough estimate of σ_c for cleavage planes by assuming a sinusoidal shape for the attractive portion of the σ versus δ curve. The analogous approximation for a grain boundary is illustrated in Fig. 8-c.

where the tensile stiffness of the grain boundary bonding is usually assumed to equal the bulk value of Young's modulus, E. These approximations yield Eq. (7).

$$\sigma_{co} \simeq \left[\frac{E\,\phi_c^*}{2\delta_o}\right]^{1/2} \tag{7}$$

It should be emphasized that Eq. (7) provides only a rough estimate of σ_c, particularly if effects of segregation are to be considered. For example, Eq. (7) implies that a decrease in ϕ_c^* (perhaps as a result of segregation) will result in a decrease in σ_{co}. If the nature (e.g., stiffness or length of interaction) of interatomic bonding changes, however, it is possible that a decrease in ϕ_c^* could be associated with an increase in σ_c. Comparison of Figs. 8-a and -b with Figs. 8-d and -e shows how such an effect might occur. Changes of this type in ϕ versus δ, and σ versus δ curves as a result of segregation might be expected if the nature of the bonding at the grain boundary changes from metallic to covalent, for example. Unfortunately, theory of interatomic bonding at structurally and chemically disturbed defects (e.g., segregated grain boundaries) is only just beginning to receive attention (31).

Interatomic Bonding: Much of the previous discussion has made use of ϕ versus δ, or σ versus δ curves, with the implicit assumption that the same curves are appropriate for pairs of atoms (e.g., A-A or A-B pairs) both on the bulk and at a grain boundary. This assumption sneaks in the back door along with the empirical observation that most pure polycrystalline metals do not fail intergranularly, hence the metallic bonding of the perfect crystal is assumed not to be seriously affected by the structural disorder associated with grain boundaries. It is not at all clear that such an assumption is valid for a grain boundary containing a significant concentration of solute however.

Losch (31) has recently suggested that the disruption in crystal periodicity and composition associated with a segregated grain boundary may significantly alter the nature of interatomic bonding in that region. Theoretical studies of sulfur bonding to nickel atom clusters are cited (32), which indicate that the Ni-S bond on a free surface is predominately S(3p)-Ni(4s), as opposed to Ni(4s)-Ni(4s) metallic bonding in the remainder of the crystal. The Ni-S bonds are localized and directional, implying covalent character. Losch also states that formation of these covalent bonds will disrupt neighboring Ni-Ni bonds.

Arguing that interatomic bonding at grain boundaries and free surfaces will be similar, Losch suggests that similar effects can be expected when sulfur (or some other metalloid element) segregates to grain boundaries in metallically bonded materials. No detailed mechanism for grain boundary crack propagation is discussed, however, the combination of strong directional covalent bonds and weakened neighboring Ni-Ni bonds is suggested to play a major role in segregation induced embrittlement.

Considerations such as these cast doubt on the assumption that any effects of segregation on ϕ_c^* will produce only a proportionate change in σ_c (12). Indeed the stiffness and directionality associated with covalent bonding might well give rise to significant changes in the shape of the σ versus δ curves of Fig. 8. Unfortunately there is neither sufficient experimental data nor theoretical analysis to indicate whether there is any predictive capacity in this new approach.

Machlin (66) has suggested an alternate explanation for segregation induced embrittlement that also involves a change in the nature of interatomic bonding at segregated grain boundaries. He argued that segregated metalloid elements form a two dimensional grain boundary phase, having at

least one elastic constant nearly equal to zero. The existence of such a phase could then result in a large elastic stress concentration at the boundary, resulting in brittle grain boundary fracture at low applied stresses.

Perfectly Brittle Grain Boundary Cracks: The "Griffith Criterion" is a necessary condition for brittle crack propagation. In its most general sense, the Griffith criterion simply states that unstable crack propagation must be associated with a net decrease in the potential energy of the stressed body (20). Griffith originally considered an isotropic, homogeneous, linearly elastic continuum having a sharp elliptical crack of/length, a, and a uniform applied stress, σ_A, normal to the crack plane and applied at boundaries far removed from the region of the crack (see Fig. 9). The appropriate form* of the Griffith criterion for/a grain boundary crack is given in Eq. (8) (60).

half

such

$$\sigma^*_{AG} = \left[\frac{\phi^*_c E}{\pi a (1 - \nu^2)}\right]^{1/2} \qquad (8)$$

where, ν is Poissons ratio and σ^*_{AG} is the critical value of the applied stress, σ_A, according to the Griffith criterion. For $\sigma_A > \sigma^*_{AG}$, the crack will propagate, and for $\sigma_A < \sigma^*_{AG}$ the crack will tend to heal in order to reduce surface energy.

---

*Equation (8) assumes that plane strain conditions are satisfied. This condition will be assumed throughout this paper.

The Griffith criterion, Eq. (8), can be rearranged to yield an expression for ϕ_c^*.

$$\phi_c^* = \frac{(\sigma_{AG}^*)^2 \pi a \ (1-\nu^2)}{E} \qquad (9)$$

For perfectly brittle crack propagation, this equation allows ϕ_c^* to be calculated from the experimentally observed fracture stress, σ_{AG}^*, crack length and elastic constants. A few studies of both cleavage and grain boundary crack propagation appear to have been carried out under conditions where the amount of crack tip plasticity was small. These studies yielded values for ϕ_c^* that approximately equal values obtained from theoretical models or thermodynamic measurements of the surface and grain boundary energies (46,6,7,13,61,62).

Being essentially an energy balance, the Griffith criterion is a necessary, but not sufficient, condition for brittle crack propagation. It takes no explicit

account of the interatomic separations occuring at the crack tip. In order to separate atoms at the crack tip, the local stress must be greater than σ_c.

Inglis (25) estimated the local tensile stress, $\sigma_{yy}(\rho)$, at the tip of an elliptical crack having a crack tip radius, ρ, (see Fig. 10) as:

$$\sigma_{yy}(\rho) = \sigma_A\left(\frac{a}{\rho}\right)^{1/2} \tag{10}$$

The critical applied stress, σ^*_{AC}, at which $\sigma_{yy}(\rho) = \sigma_c$ is given by Eq. (11).

$$\sigma^*_{AC} = \left(\frac{\rho}{a}\right)^{1/2} \sigma_c \tag{11}$$

Substituting the Orowan expression, Eq. (7), for σ_c yields Eq. (12)

$$\sigma^*_{AC} \approx \left[\left(\frac{E\gamma^*_c}{a}\right)\left(\frac{\rho}{2\delta_o}\right)\right]^{1/2} \tag{12}$$

Comparison of Eq. (12) with Eq. (8) indicates that $\sigma^*_{AG} \approx \sigma^*_{AC}$ when $\rho \approx \delta_o$, i.e. the Griffith and Orowan approaches yield approximately the same values for the critical applied stress when the crack is atomically sharp. For cracks with ρ significantly greater than δ_o, the criterion expressed in Eqs. (11) and (12) will l crack propagation, and $\sigma^*_{AC} > \sigma^*_{AG}$.

The development of Eqs. (8), (10) and (12) is based on the assumption that the material surrounding a brittle grain boundary crack is linearly elastic. Consideration of Fig. 8, on the other hand, indicates that the behavior will be highly non-linear at stresses on the order of σ_c. Barenblatt (21) has

addressed the question of nonlinear interatomic forces in the crack tip region, and concluded that a crack of the shape shown in Fig. 10 provides a more realistic view of brittle cracking than does the elliptical crack in Fig. 9. This view is reinforced by conceptual difficulties associated with the requirement that a crack tip radius, ρ, for brittle crack propagation be on the order of atomic dimensions.

Barenblatt divided the crack plane into three regions as indicated in Fig. 10: (a) the linearly elastic region away from the crack tip; (b) the "cohesive" region where interatomic forces are large, but nonlinear; and (c) the free surface region where the crack surfaces are separated sufficiently to be considered noninteracting free surfaces. For the case where the extent of the cohesive region is small compared to the total crack length, Barenblatt concluded that the shape of the crack tip region depends only on the form of the interatomic potentials, and not upon external stresses and crack length. This, in turn, allowed him to develop an expression for the critical applied stress for crack propagation, which is identical to the Griffith criterion, Eq. (8). Thus, to the extent that Barenblatt's analysis is valid, the nonlinearity of interatomic interactions at the crack tip does not seriously affect the validity of the Griffith criterion for atomically sharp cracks.

While much of the forgoing discussion has relied on the conceptual use of interatomic force laws of the type shown in Fig. 8, the analyses leading to Eqs. (8) through (12) have implicitly assumed that interatomic forces are uniformly distributed over the separating atomic planes, perhaps making "interplaner" forces a more accurate description of the manner in which they have been used.* Thomson and coworkers (18,19), using a truncated linear spring model of interatomic forces, have shown that the existence of discrete interatomic bonds across the crack plane results in a lattice trapping effect that cannot be predicted by continuum approaches. They predict a range of applied stresses, $\sigma^*_{A-} < \sigma_A < \sigma^*_{A+}$, where the crack is trapped, and cannot increase or decrease in length. For $\sigma_A > \sigma^*_{A+}$ the crack propagates, and for $\sigma_A < \sigma^*_{A-}$ the crack spontaneously heals. The Griffith stress, σ^*_{AG}, falls between σ^*_{A-} and σ^*_{A+}, and for the example given by Hsieh and Thomson (19), is closer to σ^*_{A-} then to σ^*_{A+}. Using a Griffith type equation to calculate effective cohesive energies (ϕ^*_{c-} and ϕ^*_{c+}) from σ^*_{A-} and σ^*_{A+}, they obtain $\phi^*_c \approx 1.2\phi^*_{c-} \approx 0.2\ \phi^*_{c+}$, where ϕ^*_c is the thermodynamic value of cohesive energy defined as in Eq. (6).

*This distinction would be important if numerical calculations were being performed on the basis of these force laws. Because "interplanar" and "interatomic" force laws derive from the same physical phenomena, it is assumed that any differences in shape will be small, and beyond the scope of this paper.

Hsieh and Thomson note that the degree to which lattice trapping is important increases strongly as the width of the cohesive region at the crack tip decreases. Their truncated linear spring model results in a cohesive region containing a single atomic bond, and hence represents an upper limit for lattice trapping effects. Their major conclusion, however, is that σ^*_{AG}, as expressed in Eq. (8), may be significantly less than the actual applied stress, σ^*_{A+}, required to propagate a brittle crack in a discrete lattice.

The effects of segregation on brittle crack propagation can manifest themselves in at least three ways. The effect of segregation on ϕ^*_c [Eq. (6)]will clearly influence σ^*_{AG} according to Eq. (8). The results in Table II and Fig. 7 indicate that grain boundaries in pure iron have ϕ^*_c of about 3.4 J/m^2. For a Griffith type crack about 10 μm long, Eq. (8) predicts $\sigma^*_{AG} \simeq 158$ MPa for pure iron. As the bulk phosphorus content of the iron increases, ϕ^*_c approached a value of about 3.1 J/m^2, and for the same 10 μm Griffith crack, $\sigma^*_{AG} \simeq 150$ MPa. The modest changes in fracture stress indicated by these values do not appear to explain the rather dramatic decreases in strength and ductility normally associated with segregation induced embrittlement of grain boundaries. While the decrease in ϕ^*_c may contribute to embrittlement, it alone does not appear to explain it.

To the extent that Orowan expression for σ_c is accurate, changes in σ_c resulting from solute segregation will affect σ^*_{AC} to approximately the same extent that it affects σ^*_{AG}. As pointed out in the foregoing discussion, however, changes in the nature of interatomic bonding at grain boundaries as a result of solute segregation may invalidate some of the assumptions used in obtaining Eq. (7) and hence Eq. (12). Equation (11) indicates that σ^*_{AC} is directly proportional to, and hence more strongly dependent upon, σ_c than ϕ^*_{AG} is upon ϕ^*_c.

Finally, the lattice trapping effect discussed by Thomson and coworkers (18,19) will be strongly dependent upon the shape of the interatomic force separation curve, and the extent to which bonding is localized between individual atoms (as in covalent bonding), or distributed uniformly (as in the free electron gas model of metallic cohesion).

Nearly Brittle Grain Boundary Cracks:

Grain boundary fracture in metals, at temperatures significantly above absolute zero, nearly always involves at least some plastic deformation. Figures 1 and 2 show evidence of significant plastic deformation associated with grain boundary crack propagation. The extent of plastic deformation varies with temperature, strain rate, and material, often resulting in elongations of several percent.

Unfortunately, there have been few detailed studies of plastic deformation associated with grain boundary fracture, so our view of the mechanistic details must largely be inferred from macroscopic mechanical test results.

General yielding (often in the microstrain range) of unnotched polycrystalline materials is expected to play a major role in the nucleation of grain boundary cracks. Local stresses, significantly greater than the nominal applied stress, can be generated by various mechanisms involving inhomogeneous plastic deformation. It seems likely that the previously outlined effects of segregation on ϕ_c^* and σ_c will affect the local stress intensity required for nucleation of a grain boundary crack. Except for this observation, nucleation (as opposed to growth) of grain boundary cracks will not be explicitly considered in this paper. For an overview of crack nucleation in nearly brittle materials, the reader is referred to the work of Lawn and Wilshaw (27).

General yielding is not expected to play a major role in grain boundary crack propagation, except in that work hardening will permit applied stresses greater than the yield stress to be achieved. In the following discussion, only plastic deformation in the immediate vicinity of the crack tip is

considered. The principle aspects of crack tip plasticity are illustrated schematically in Fig. 11.

Crack tip plasticity plays at least four major roles in crack propagation. First, plastic deformation requires mechanical work to be performed, which expends a portion of the stored elastic strain energy that would otherwise be available for breaking interatomic bonds at the crack tip. Secondly, plastic deformation will tend

to relieve the stress intensity at the crack tip, resulting in higher values of σ_A to achieve a crack tip stress equal to the cohesive stress. A related effect is associated with crack blunting in which dislocations created at the highly stressed crack tip increase the crack tip radius, ρ. Thirdly, plastic deformation, being an inherently irreversable phenomenon, virtually eliminates the possibility of spontaneous crack healing of the type expected for perfectly brittle cracks.* Finally, plastic deformation may be responsible for creating a region of high uniaxial tension ahead of the crack. These four roles will be discussed in the following paragraphs, and where possible, effects of solute segregation will be included in the discussion.

---

*Crack tip plasticity does not necessarily preclude healing of cracks by thermally activated processes, e.g. sintering.

Orowan (15,22) and Irwin (38) extended the Griffith approach to the case of nearly brittle crack propagation. They postulated a characteristic fracture energy, ϕ_f, that is related to the fracture stress, σ^*_{A0}, by an equation analogous to Eq. (7).

$$\sigma^*_{A0} = \left[\frac{\phi_f E}{\pi\, a(1-\nu^2)}\right]^{1/2} \tag{13}$$

The fracture energy, ϕ_f, is generally assumed to be the sum of ϕ^*_c and ϕ_p (plastic work per unit area). This approach assumes that ϕ_f can be treated as a material property, allowing Eq. (13) to be rearranged to yield an expression for ϕ_f analogous to Eq. (9).

$$\phi_f = \frac{\sigma^{*2}_{A0}\, \pi\, a(1-\nu^2)}{E} \tag{14}$$

Equation (14) allows ϕ_f to be calculated from experimentally observable quantities and is essentially equivalent to the critical strain energy release rate, G_{IC}, of linear elastic fracture mechanics.

Thompson and co-workers (6,7) have studied the fracture of notched Fe + 3% Si bicrystals, doped with various levels of phosphorus. Figure 12 shows a plot of ϕ_f versus absolute temperature, T, for bicrystals containing 0.12 wt % phosphorus. Perhaps fortuitously, as T approaches zero,

ϕ_f approaches a value in the range 2.5–3.0 J/m^2, surprisingly close to the values of ϕ_c^* plotted in Fig. 7 (calculated using Hondros' data). These same authors also reported values of ϕ_f plotted versus phosphorus concentration at the grain boundaries, for bicrystals fractured at 77 K, as shown in Fig. 13. Qualitatively similar effects of segregation on G_{IC} have been reported by Mulford for 3340 steel embrittled by antimony and phosphorus segregation.*

Comparison of the effect of segregation on ϕ_c^* (Fig. 7), with its effect on ϕ_f (Fig. 13) indicates that segregation is affecting ϕ_f through other mechanisms than the effect on ϕ_c^* indicated in Fig. 7. To the extent that $\phi_f \approx \phi_c^* + \phi_p$, the experimental data in Figs. 12 and 13 indicate that segregation is having a direct effect upon ϕ_p. McLean (28) has suggested that ϕ_c^* acts as a kind of "valve" directly controlling the amount of plastic deformation associated with nearly brittle crack propagation, and hence the value of ϕ_p. Through such a mechanism, segregation could exert a major effect on ϕ_p as a result of its relatively modest effects on ϕ_c^* already mentioned. McMahon and Vitek (12) have expanded on this idea, noting that

*Mulford's results (13) are cited by McMahon and Vitek (12).

the plastic strain rate in iron is strongly dependent upon stress. They argue that small changes in ϕ_c^* (due to segregation) will result in correspondingly small changes in σ_{eff} (the "effective" tensile stress in the region of a small propagating crack*). The strong dependence of plastic strain rate on σ_{eff}, coupled with a high crack velocity combined to explain how small changes in σ_{eff} result in large changes in ϕ_p. A similar approach to crack tip plasticity in cleavage fracture (minus the segregation effect) is described by Tetelman and McEvily (14). The treatment of McMahon and Vitek recognizes what seems to be an important factor in the relationship between segregation and ϕ_p. Their analysis neglects several other factors, however, that could also affect that relationship, especially in materials for which the stress dependence of plastic strain rate is not so strong as in iron.

McMahon and Vitek's model (12) explicitly assumes that the plastic zone thickness (R_p in Fig. 11) is approximately constant. Because ϕ_p is directly proportional to R_p, any dependence on segregation

---

*Because McMahon and Vitek were considering the transition from nucleation to growth, σ_{eff} is larger than the nominal applied stress, σ_A. Mechanisms for stress intensification include inhomogeneous plastic deformation and plastic constraint at macroscopic notches.

could be significant. If we assume that R_p is the distance from the crack tip at which some critical stress level, σ_p, can be maintained, then R_p can be approximated* as:

$$R_p = \frac{a\ \sigma_A^2\ F^2(\psi)}{2\sigma_p^2} \qquad (15)$$

where $F(\psi)$ is a function of ψ (see Fig. 9) whose exact form depends upon the component of stress referred to by σ_p (e.g., tensile or shear). The $(\sigma_A/\sigma_p)^2$ dependence of R_p is in agreement with a dislocation model (30) and with slip line field models (ref. 14, pp. 293-6) of plastic deformation at stationary cracks or notches.

Crack tip plasticity will occur in such a way as to relieve stresses at the crack tip. This in turn will require larger applied stresses to achieve a given crack tip stress intensity. One mechanism by which this can happen is via dislocation emission or adsorption at or near the crack tip. This will result in an increase in the effective crack tip radius,

---

* This approximation assumes the stress field, $\sigma(r,\psi)$ for an elliptical crack in a linear elastic continuum (ref. 14, p. 49). The solution is applicable for $\rho << R_p << a$.

and a decrease in the crack tip stress intensification [see Eq. (10)]. Recall that for $\rho >> \delta_o$, $\sigma^*_{AC} >> \sigma^*_{AG}$ and the crack tip cohesive stress becomes the factor limiting crack propagation. For a propagating crack where $\sigma_A = \sigma^*_{AC} = (\rho/a)^{1/2} \sigma_c$ [Eq. (11)] Eq. (15) can be rewritten:

$$R_p = \frac{\rho \sigma_c^2 F^2(\psi)}{2\sigma_p^2} \quad . \tag{16}$$

According to McMahon and Vitek, ϕ_p is proportional to R_p, hence ϕ_p is proportional to ρ, σ_c^2 and σ_p^{-2}.

If the weak, $\phi_c^{*1/2}$ dependence of σ_c indicated in Eq. (7) is assumed, then ϕ_p is proportional to ϕ_c^*; a significant, but not overwhelming effect in light of the previously discussed dependence of ϕ_c^* on segregation. As previously noted, however, Eq. (7) provides only a rough estimate of σ_c, and the $\phi_c^{*1/2}$ dependence of σ_c is based on the assumption that the shape of the σ versus δ curve (Fig. 8-a) remains constant as $\phi_c^{*1/2}$ is changed (e.g., via segregation).

The above discussion centers primarily on the effect of segregation on the crack tip stress field as the driving force for crack tip plasticity. The questions of how the dislocations necessary for this plastic deformation are created, and how segregation might affect their creation, are not addressed. There are at least two possible sources for dislocations near a crack tip. First, dislocations can be generated at sources within the adjacent grains, lying close enough to the boundary to be activated as the crack tip passes. Because of the extreme thinness of the segregated region at the boundary, it seems unlikely that grain boundary segregation will have any direct effect on these internal sources.*

*The same solute species that segregate strongly to grain boundaries are also likely to segregate to internal crystal defects that act as dislocation sources. To this extent, internal sources could be affected by the presence of a segregating solute species. Any effect of these solutes on crack tip plasticity, however, would be similar for both transgranular and intergranular cracks.

A second mechanism for generating the dislocations involved in crack tip plasticity is nucleation at the crack tip. Mason (69) has applied a model for crack tip dislocation nucleation, originally developed by Rice and Thomson (68), to the case of grain boundary cracks in copper embrittled by bismuth. This model considers the competing processes of Griffith type crack propagation, and punching of dislocations from the crack tip. Mason considered two effects of segregation, the first being the lowering of ϕ_c and the other the lowering of γ_{step} (the energy of the step or ledge left behind at the crack tip after nucleation of the dislocation loop.*) The results of her analysis indicate that dislocations can be nucleated on significantly fewer slip systems in the segregated boundaries than for boundaries in pure copper.

---

*Mason noted that ϕ_c^* is really the appropriate cohesive energy, but used equilibrium values of ϕ_c and γ_s in her analysis of the Cu-Bi system.

Summary

Attempts to veiw intergranular fracture as Griffith type crack propagation, with the effects of segregation entering only through its influence on ϕ_c^* is clearly unable to explain the vast majority of experimental observations. The thermodynamic analyses of Hirth and Rice (5) show that for solute species which segregate more strongly to free seufaces than to grain boundaries, the cohesive energy of the boundary is lowered. The experimental data of Hondros (1) suggests taht the decrease in ϕ_c^* associated with phosphorus segregation in iron at 1450°C is on the order of 10% (2). Changes in ϕ_c^* of similar magnitude might reasonably be expected for other solute-solvent systems where strong segregation is known to occur.

The recent observations of enhanced ductility associated with segregation complicate the connection between segregation, ϕ_c^*, and intergranular fracture (51,52,53). Unfortunately, the kind of surface and grain boundary energy measurements that are available for the Fe-P system, are not available for any of these systems. This ignorance of fundamental physical properties makes it difficult to determine whether ϕ_c^* increases or decreases as a result

of beneficial segregation. Such information would be of obvious value in testing the correlation between ϕ_c^* and intergranular fracture.

The limited experimental data on intergranular fracture energies seems to indicate that (except possibly in very special cases) segregation effects on ϕ_c^* are only a small part of the story. The data of Thompson et al. (6,7), and similar data by Mulford (13), indicates that while segregation changes ϕ_c^* by ~10% (a few tenths of a J/m^2), ϕ_f may change by 1--2 orders of magnitude. Clearly, in addition to performing the reversible work associated with the separation of grain boundary atoms at the crack tip, the crack tip stress field is performing relatively large amounts of plastic work in the region near the crack tip. It is also clear that in order to explain segregation induced intergranular fracture, segregation of embrittling solutes must be significantly reducing crack tip plasticity. It is the mechanism by which segregation affects crack tip plasticity that is unresolved at the present time.

Crack tip plasticity occurs under the influence of the crack tip stress field, as the crack propagates along the boundary. To the extent that the crack tip stress field must also separate atoms, its intensity will reflect

the cohesive strength of the grain boundary. Equation (6) suggests a rather weak dependence of σ_c^* on ϕ_c^*, and hence a weak dependence on segregation. McMahon and Vitek (12) have suggested (in the case of iron base alloys at least) that this weak dependence of σ_c on segregation may be significantly enhanced by the strong dependence of plastic strain rate on stress. Similar explanations may hold for other metals, however in copper the dislocation velocity is reported to be only weakly dependent on stress (70) suggesting that segregation induced embrittlement in the Cu-Bi system, for instance, might not be similarly explained. Mason (69), on the other hand, suggests that crack tip plasticity in the Cu-Bi system may be controlled through the effect of segregation on dislocation nucleation at the crack tip.

The dependence of ϕ_c^* on segregation, as indicated in Eq. (5), is firmly based in equilibrium thermodynamics, and contains a minimum set of arbritrary assumptions. The dependence of σ_c on segregation, however, cannot be easily estimated from equilibrium thermodynamic quantities. While ϕ_c^* and σ_c are generally assumed (12) to vary in a similar way with segregation [as implied by Eq. (6)], the considerations illustrated in Fig. 8 suggest that this assumption might not always be valid. The attempt by Losch (31), and to

some extent by Machlin (66), to explain segregation induced embrittlement by considering the details of interatomic bonding between specific solute and solvent species is clearly an important contribution to the overall picture of segregation induced embrittlement. It would be useful, for instance, if a beneficial segregant, and a harmful one, could be studied for the same base metal. There is some eivdence that boron might be such a beneficial segregant in iron (33), to complement the fairly extensive study of phosphorus in iron as a harmful segregant. If confirmed experimentally, it would be most interesting to see if cluster model calculations, elastic moduli of bulk Fe-P and Fe-B compounds, and thermodynamic estimates of ϕ_c^* could predict (even qualitatively) the beneficial versus harmful effects of the two solutes.

Acknowledgments

This study was supported by the Division of Materials Sciences, Office of Basic Energy Sciences, U.S. Department of Energy under contract W-7405-eng-26, with Martin Marietta Laboratories, Baltimore Research Laboratory.

The author would like to express appreciation to M. H. Yoo for discussion and comments on the manuscript and to S. P. Buhl for typing the manuscript.

Table I. Alloy-Trace Impurity Combinations Resulting in Segregation and Embrittlement

Alloy	Impurity	Ref.
Fe	P, S, Te	34, 37
Fe + 3% Si	P	6, 7
Low alloy (Ni, Cr) steel	P, Sb, Sn	39
Ni	S	40
Cu	Bi, Sb, Te, S	26, 41, 42, 43
Mo	O	46
W	P	44
Ir + 0.3% W	P	50
Ni_3Al	S	47
Ni-Al-Ti	S	45
Pt + 30Rh + 8W	Se	48
Cu + 3Al + 1Si	Pb	49

Table II. Calculated Values of Cohesive Energy for Three Levels of Phosphorus in δFe at 1450°C*

$\log X_P'$	−1.5	−1.0	−0.5
X_P (at. %)	0.032	0.100	0.320
γ^s $(\frac{erg}{cm^2})$	1960	1750	1420
γ^b $(\frac{erg}{cm^2})$	.760	.673	.500
$\phi_c = 2\gamma^s - \gamma^b$	3160	2827	2340
$\Gamma^s_{P(Fe)}$ $(\frac{g \cdot atom}{cm^2})$	6.5×10^{-10}	18.5×10^{-10}	21.4×10^{-10}
$\Gamma^b_{P(Fe)}$ ( )	2.2×10^{-10}	8.3×10^{-10}	10.7×10^{-10}
$\Gamma_P^{sH} = 1/2\ \Gamma_P^b$	1.1	4.15	5.35
X_P^H	.00615	0.02186	.0265
γ^{sH}	2060	2000	1980
ϕ_c^*(Seah) $= 2\gamma^{sH} - \gamma^b$	3360	3327	3460
ϕ_c^*(H-T)	3308	3146	3080

*From the data of Hondros, ref. 1.

References

1. E. D. Hondros, "The Influence of Phosphorus in Dilute Solid Solution on the Absolute Surface and Grain Boundary Energies of Iron", Proc. R. Soc. A, 286, 479-498 (1965).

2. R. J. Asaro, "Adsorption Induced Losses in Interfacial Cohesion", Proc. R. Soc. A, 295, 151-163 (1980).

3. M. P. Seah, "Segregation and the Strength of Grain Boundaries", Proc. R. Soc. A, 349, 535-554 (1976).

4. J. P. Hirth, "Adsorption at Grain Boundaries and its Effect on Decohesion", Proc. R. Soc. A, 295, 139-149 (1980).

5. J. P. Hirth and J. R. Rice, "On the Thermodynamics of Adsorption at Interfaces as it Influences Decohesion", to be published.

6. R. G. Thompson, C. L. White, J. J. Wert, and D. S. Easton, "On the Mechanism of Intergranular Embrittlement by Phosphorus (in Transformer Steel), to be published.

7. R. G. Thompson, "The Role of Phos ıorus in the Intergranular Embrittlement of Fe-3Si", Ph.D. Thesis, Vanderb t University, Nashville, TN (1979).

8. D. F. Stein and J. R. Low, "Mobil y of Edge Dislocations in Silicon-Iron Crystals", J. Appl. Phys. vol 31(.), pp. 362-9 (1960).

9. J. F. Knott, "Fundamentals of Fracture Mechanics, John Wiley & Sons, New York (1973).

10. J. J. Gilman, "Direct Measurements of the Surface Energies of Crystals", J. Appl. Phys., v-l 31 (12), pp. 2208-2218 (1960).

11. C. J. McMahon, Jr., V. Vitek, and G. R. Belton, "On the Theory of Embrittlement of Steels by Segregated Impurities", Scripta Met, vol. 12, pp 785-789 (1978).

12. C. J. McMahon, Jr., and V. Vitek, "The Effects of Segregated Impurities on Intergranular Fracture Energy", Acta Met., vol 27, pp. 507-513 (1979).

13. R. A. Mulford, Ph.D. Thesis, University of Pennsylvania (1974) referenced in[12].

14. A. S. Tetelman and A. J. McEvily, Jr., Fracture of Structural Materials, John Wiley and Sons, New York (1967), pp. 208-212.

15. E. Orowan, Rep. Prog. in Phys., vol 12, p. 185 (1948-9).

16. M. Polanyi, Z. Phys., 7, pp. 323 (1921).

17. R. M. Thomson, "The Fracture Crack as an Imperfection in a Nearly Perfect Solid", in Ann. Rev. of Materials Sci. vol 3, R. A. Huggins, editor, pp. 31-51 (1973).

18. R. M. Thomson, C. Hsieh, and V. Rana, J. Appl Phys., vol 42 (8), pp. 3154-3160 (1971).

19. C. Hsieh and R. Thomson, J. Appl. Phys., vol 44 (5), pp. 2051-2063 (1973).

20. A. A. Griffith, Phil. Trans. Roy Soc., vol 221, pp. 163-198 (1920).

21. G. I. Barenblatt, "The Mathematical Theory of Equilibrium Cracks in Brittle Fracture", in Advances in Applied Mechanics, vol 7, H. L. Dryden and Th. von Kármán, editors, Academic Press, New York (1962) pp. 55-129.

22. E. O. Orowan, "Fundamentals of Brittle Behavior of Metals" in Fatigue and Fracture of Metals, edited by W. M. Murray, pp. 139-167, Wiley, New York (1950).

23. D. K. Felbeck and E. Orowan, "Experiments on Brittle Fracture of Steel Plates", Weld. Res. Suppl., vol 34, pp. 570s-575s, (1955).

24. D. D. Mason, Masters Thesis, Brown University.

25. C. Anglis, Inst. Nav. Architecture, LV: 219 (1913).

26. E. D. Hondros and D. McLean, "Cohesion Margin of Copper", Phil. Mag., vol 29 pp. 771-95 (1974).

27. B. R. Lawn and T. R. Wilshaw, Fracture of Brittle Solids, Cambridge Universit Press, Cambridge (1975).

28. D. McLean, Mechanical Properties of Metals, John Wiley & Sons, New York (1962), pp. 249-250.

29. J. Friedel, "Propagation of Cracks and Work Hardening", in Fracture, B. L Averback et al, editors, John Wiley & Sons (1959) pp. 498-523.

30. J. E. Sinclair, "A Dislocation-Based, Geometrically Consistent, Model of Plasticity in Fracture", Nucl. Metall, vol. 20, pp. 388-404 (1976).

31. W. Losch, "A New Model of Grain Boundary Failure in Temper Embrittled Steel", Acta Met. vol 27, pp. 1885-1892 (1979).

32. S. P. Walch and W. A. Goddard III, "Theoretical Studies of the Bonding of Sulfur to Models of the (100) Surface of Nickel", Surf Sci, vol 72, pp. 645-677 (1978).

33. H. (Hidetake) Taga and A. (Akiyoshi) Yoshikawa, "Effect of Boron on Grain Boundary Strength of Iron", Proc. ICSTIS, Suppl. Trans. ISIJ, vol 11, pp. 1256-1259 (1971).

34. C. J. McMahon, Jr. and L. Marchut, "Solute Segregation in Iron-Based Alloys, J. Vac. Sci. Technol., vol 15 (2), pp. 450-466 (1978).

35. K. Monma and H. Suto, "Effects of Dissolved Sulfur on the Surface Tension of Iron, Cobalt and Nickel Saturated with Carbon", Jap. Inst. Metals. Journal, vol 24, pp. 611-614 (1960).

36. A. C. Yen, W. R. Graham, and G. R. Belton, "The Segregation of Phosphorus to the Free Surface of a Ferritic Iron Alloy at 723 to 823 K", Met Trans A, vol 9A, pp. 31-34 (1978).

37. P. V. Ramasubramanian and D. F. Stein, Met. Trans., vol 4, pp. 1735-1742 (1973).

38. G. Irwin, Trans ASM, (1947), p. 147.

39. A. Joshi and D. F. stein, "Temper Embrittlement of Low Alloy Steels", ASTM-STP 499, pp. 59-89 (1972) ASTM, Philadelphia, PA 19103.

40. A. W. Thompson, "Effect of Sulfur Segregation to Grain Boundaries on Yielding, Flow, and Fracture of Nickel", in Grain Boundaries in Engineering Materials, Proc. of the 4th Bolton Landing Conf. June 1974, J. L. Walter et al, editors, Claitors Publ. Div., Baton Rouge (1975) pp. 607-618.

41. H. L. Marcus and N. E. Paton, Met. Trans., vol 5, pp. 2135-2138 (1974).

42. S. P. lough and D. F. Stein, Scripta Met.. vol 9, pp. 1163-1166 (1975).

43. V. I. Arkharov, Ye. S. Markhasin, and Z. A. Samoylenleo, Fiz. Metal. Metalloved., vol 29 (5), pp. 987-991 (1970).

44. A. Joshi and D. F. Stein, Met. Trans., vol 1, pp. 2543-2546 (1970).

45. W. C. Johnson, J. E. Doherty, B. H. Kear, and A. F. Giamei, Scripta Met, vol 8, pp. 971-974 (1974).

46. A. Kumar and B. L. Eyre, Proc. R. Soc. Lond. A, vol 370, pp. 431-458 (1980).

47. C. L. White and D. F. Stein, Met. Trans. A, vol. 9A, pp. 13-22 (1978).

48. C. L. White, J. R. Keiser, L. Heatherly, and J. F. Newsom, Scripta Met., vol 13, pp. 543-547 (1979).

49. C. L. White, T. R. Odom and R. E. Clausing, "A Study of Grain Boundary Embrittlement in Cu-3Al-1Si Using AES", accepted for publication in the proceedings of the 12th International Metallographic Society Technical Meeting.

50. C. L. White and C. T. Liu, Scripta Met., vol 12, pp. 727-733 (1978).

51. C. L. White, R. E. Clausing and L. Heatherly, Met Trans A, vol 10A, pp. 683-691 (1979).

52. C. L White, J. R. Keiser, and D. N. Braski, "Boron Segregation to Grain Boundaries and Improved Ductility in Pt + 30 wt % Rh + 8 wt. % w", unpublished research, to be submitted to Met. Trans.

53. S. K. Hwang and J. W. Morris, Jr., Met. Trans., Vol. 11A, pp. 1197-1206 (1980).

54. D. McLean, GrainBoundaries in ... als, Oxford, Clarendon Press, London (1957), pp. 116-149.

55. M. P. Seah and E. E. Hondros, Proc. R. Soc. Lond. A, vol 335, pp. 191-212 (1973).

56. E. D. Hondr..., "Energetics of Solid-Solid Interfaces", in Interfaces Conferen..., R. C. Gifkins, editor, Butterworths, Sydney (1969), pp. 77-100.

57. R. Defay, I. Prigogiue, A. Bellemans, and D. H. Everett, Surface Tension and Adsorption, Longmans, London (1966) pp. 85-94.

58. J. W. Gibbs, The Scientific Papers of J. Willard Gibbs, vol I, Dover, New York (1961), pp. 219-331.

59. C. L. White and W. A. Coghlan, Met. Trans A, vol 8A, pp. 1403-1412 (1977).

60. A. S. Tetelman and A. J. McEviley, Jr., pp. 38-85 in ref. 14.

61. J. J. Gilman, J. Appl. Phys., vol 31 (12), pp. 2208-2218 (1960).

62. J. E. Corwell and D. Hull, Phil. Mag., vol 27, pp. 1183-1192 (1973).

63. S. Brunauer, P. H. Emmett and E. Teller, J. Am. Chem. Soc., vol. 60, pp. 309-319 (1938)

64. S. Brunauer, L. S. Deming, W. E. Deming and E. Teller, J. Am. Chem. Soc. vol. 62, pp. 1723-32 (1940).

65. I. Prigogine and R. Defay (translated by D. H. Everette), Chemical Thermodynamics, Longmans Green and Co., New York (1954) pp. 332-339.

66. E. S. Machlin, Scripta Met, vol. 12, pp. 111-112 (1978).

67. E. S. Machlin and A. Levi, Scripta Met, vol. 14, pp. 127-8 (1980)

68. J. R. Rice and R. Thomson, Phil. Mag., vol 29 (1), pp. 73-97 (1974).

69. D. D. Mason, Phil. Mag., vol 39 (4), pp. 455-468 (1979).

70. W. F. Greenman, T. Vreeland Jr. and D. S. Wood, J. Appl. Phys., vol. 38 (9), pp. 3595-3603 (1967).

Figure Captions

1. Scanning electron micrograph of Ir + 0.3%W fractured intergranular y at room temperature. Note slip lines intersecting the intergranular fracture surface.

2. Scanning electron micrograph of Cu + 3% Al + 1% Si fractured intergranularly at room temperature. Note the transition from smooth intergranular fracture, to slip lines and superficial tearing.

Fig. 3. Schematic representation of a 38° <100> tilt boundary in a simple cubic crystal.

Fig. 4. Hypothetical interatomic potentials for A-A and A-B bonds.

Fig. 5. Composition, C_B, versus distance, Z, profiles across; (a) a grain boundary, (b) a free surface created by rapid fracture of the grain boundary in (a), (c) a free surface created by equilibrium separation of the grain boundary in (a), and (d) a free surface created in equilibrium with a bulk concentration C_B^H, such that $\Gamma_B^{sH} = (1/2)\,\Gamma_B^b$.

Fig. 6. (a) Experimental values of γ_s and γ_b for Fe-P alloys at 1450 C (after Hondros, ref 1).
(b) Values of Γ_p^s and Γ_p^b for the Fe-P alloys in (a), (after Hondros, ref.1)

Fig. 7. Plots of ϕ_c ϕ_c according to Seah, and ϕ^*_c according to Hirth and Rice, versus X_p for Fe. Calculations using the experimental data of Hondros (1).

Fig. 8. Hypothetical ϕ versus δ and σ versus δ curves. Comparison of (a) and (b) with (d) and (e) shows a possible effect of segregation, where $\phi^*_c < \phi^{*\prime}_c$ yet $\sigma'_c > \sigma_c$. Comparison of (c) and (f) illustrates the respective Orowan approximations to the σ versus δ curves.

Fig. 9. Schematic of an elliptical, "Griffith type" crack.

Fig. 10. Schematic of a Barenblatt type crack.

Fig. 11. Schematic of the plastic deformation associated with a propagating grain boundary crack.

Fig. 12. A plot of ϕ_f versus T for embrittles Fe + 3% Si + 0.12%P bicrystals (after Thompson, ref. 7).

Fig. 13. A plot of ϕ_f versus grain boundary phosphorus concentration for embrittled Fe + 3% Si + 0.12 %P bicrystals at 77 K.

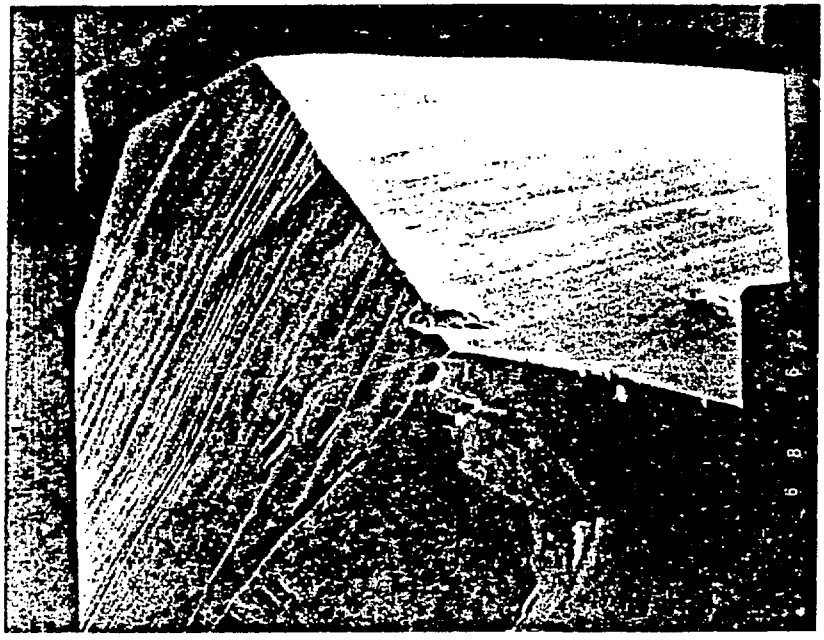

Fig. 1 Scanning electron micrograph of Ir+0.3%W fractured at room temperature. Note evidence of dislocation slip intersecting intergranular fracture surface.

Fig. 2

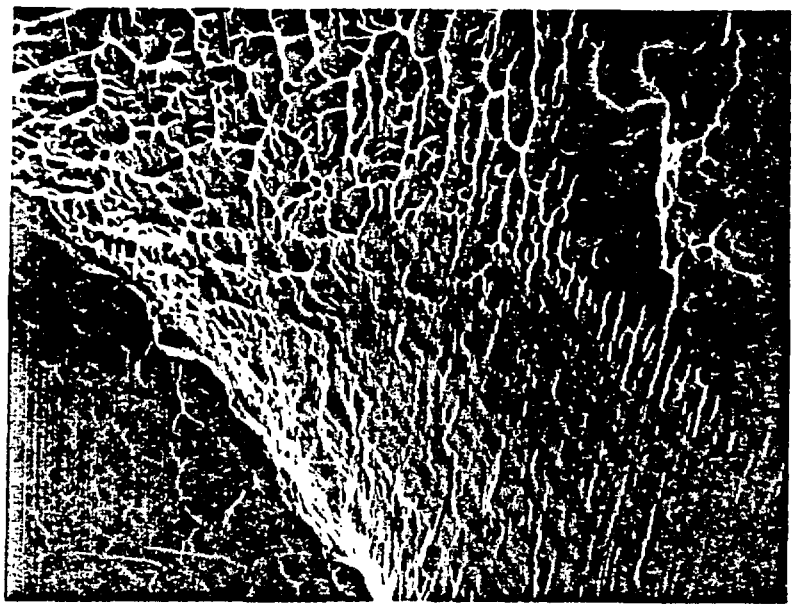

Fig. 2 Scanning electron micrograph of Cu + 3% Al + 1% Si fractured at room temperature. Note evidence of dislocation slip and ductile tearing associated with intergranular fracture.

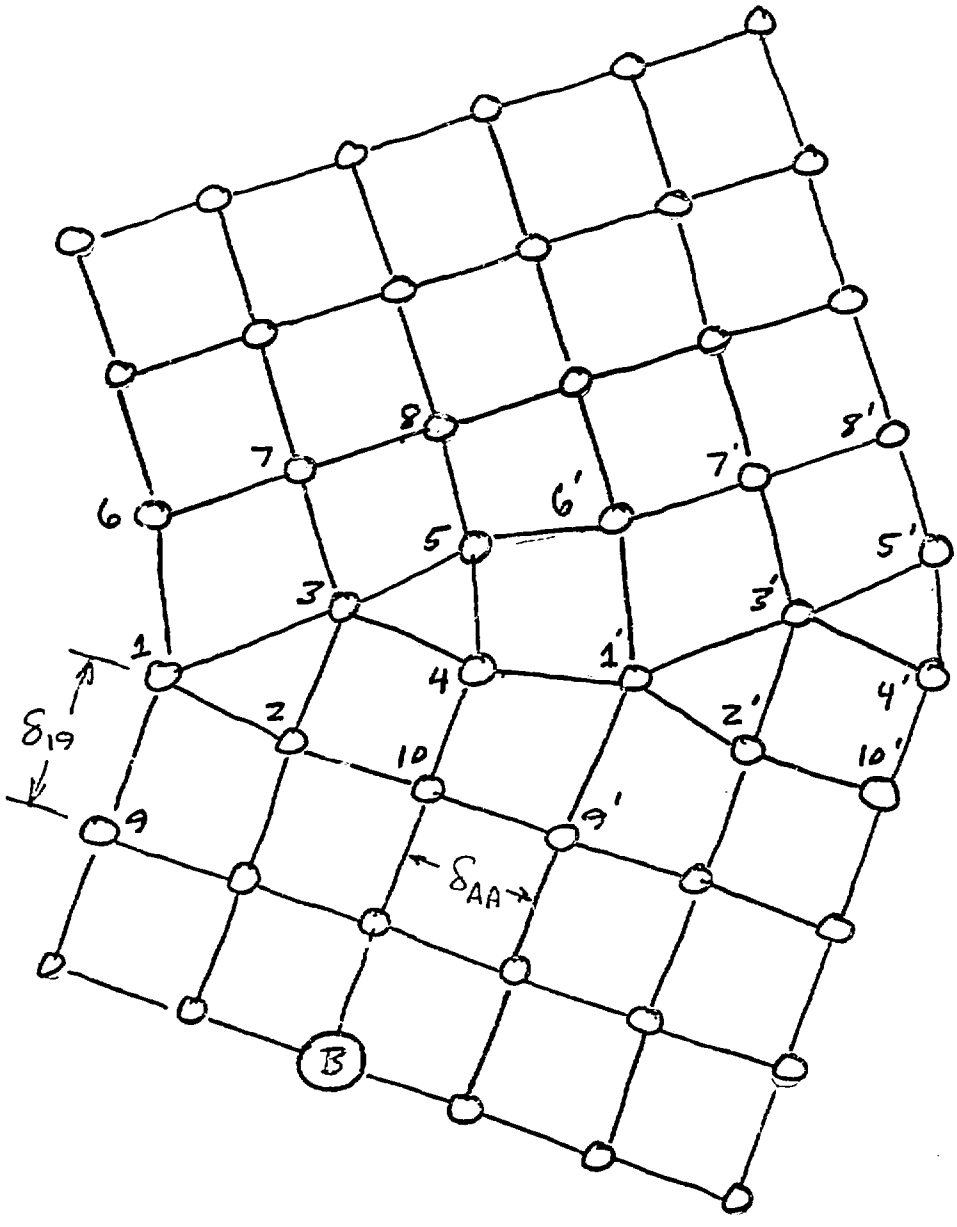

Fig. 3 Schematic representation of a 38° ⟨100⟩ tilt boundary in an fcc crystal

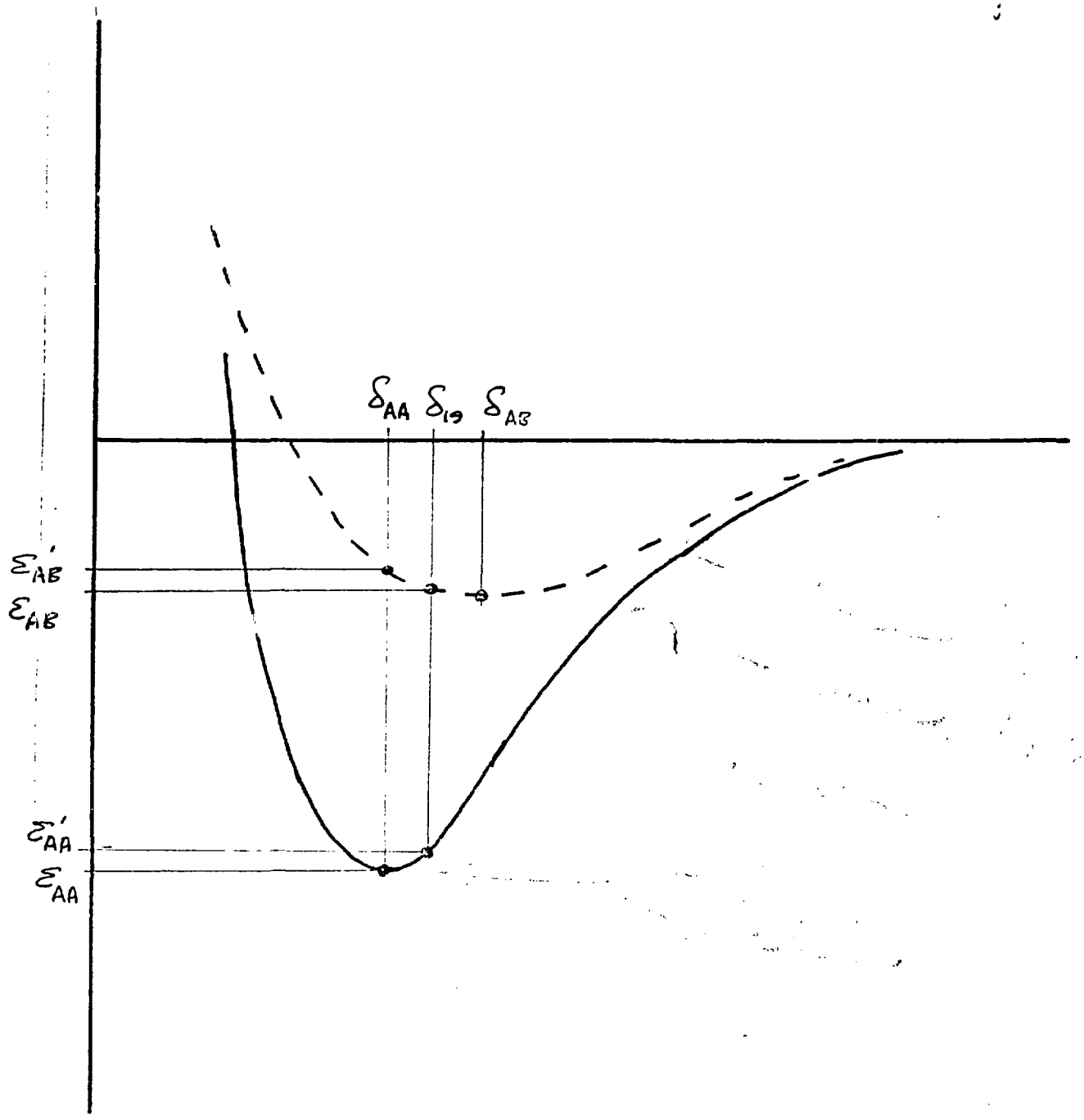

Fig. 4 Hypothetical interatomic potentials for A-A and A-B bonds

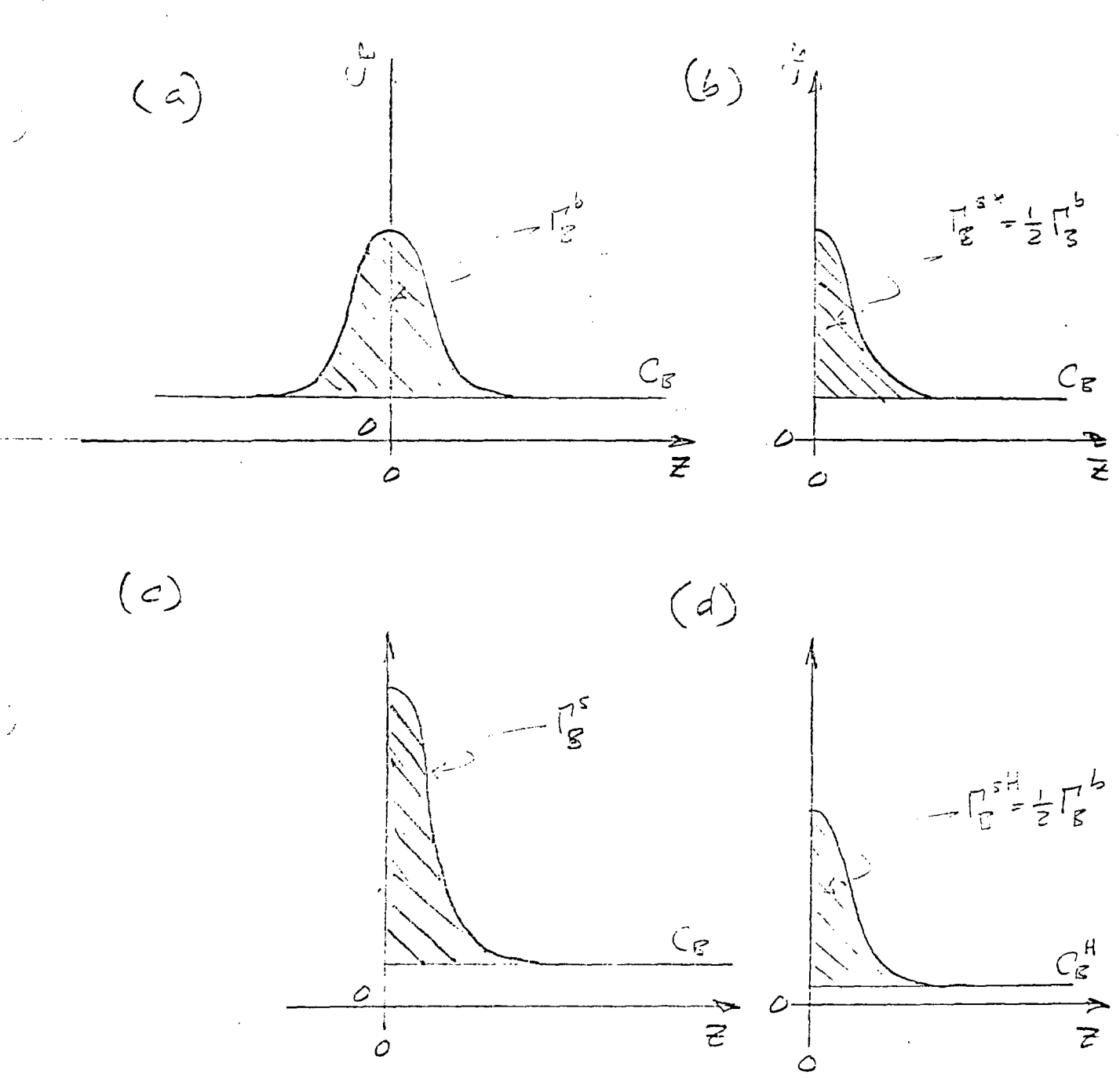

Fig. 5

Composition (C_B) versus distance (z) profiles across ~~boundaries and free surfaces~~; (a) grain boundary, (b) free surface created by rapid intergranular fracture, (c) free surface created by equilibrium

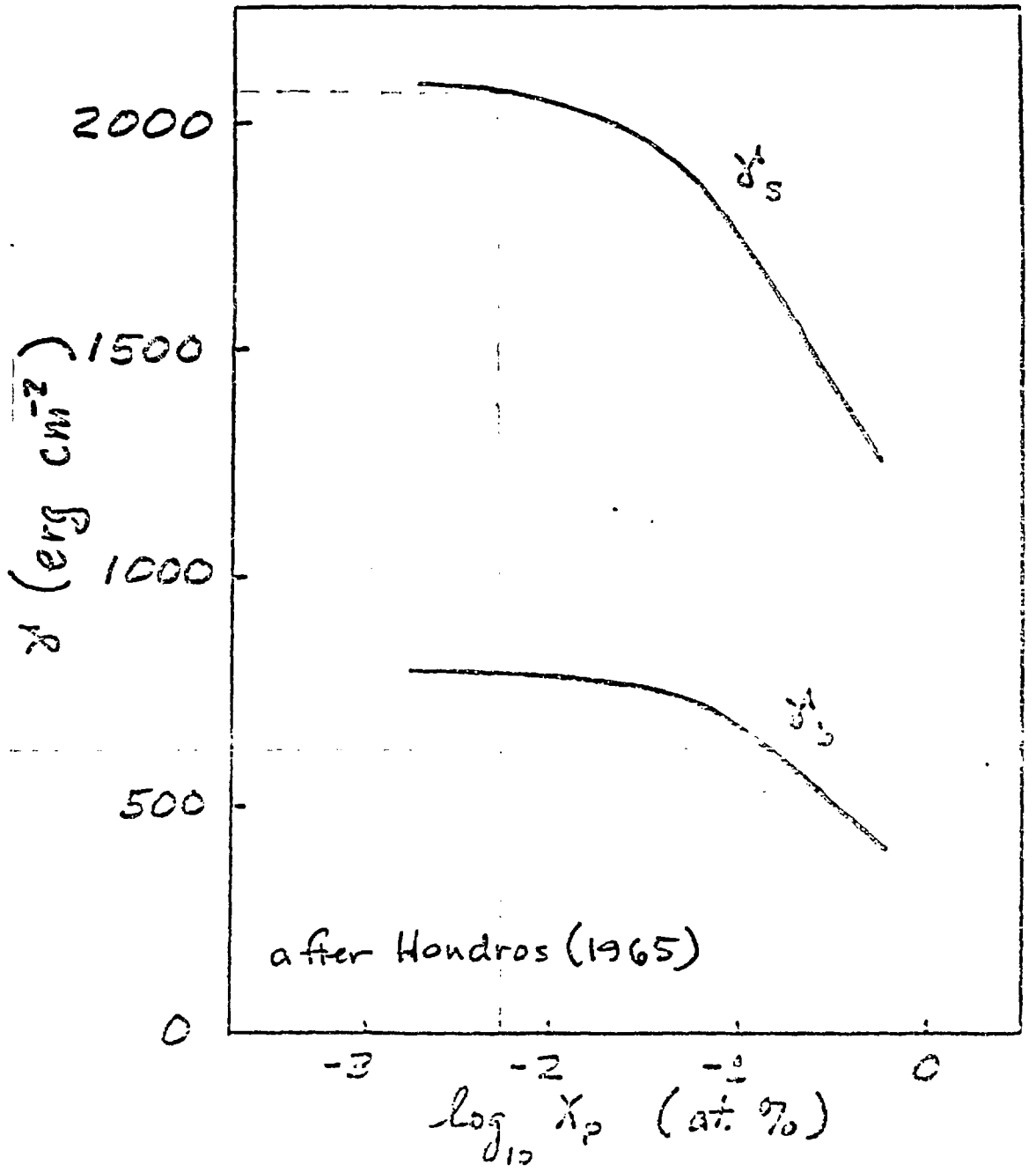

Fig. 6 (a) Experimental values of γ_s and γ_b for Fe-P alloys at 1450°C, after Hondros, ref (1).

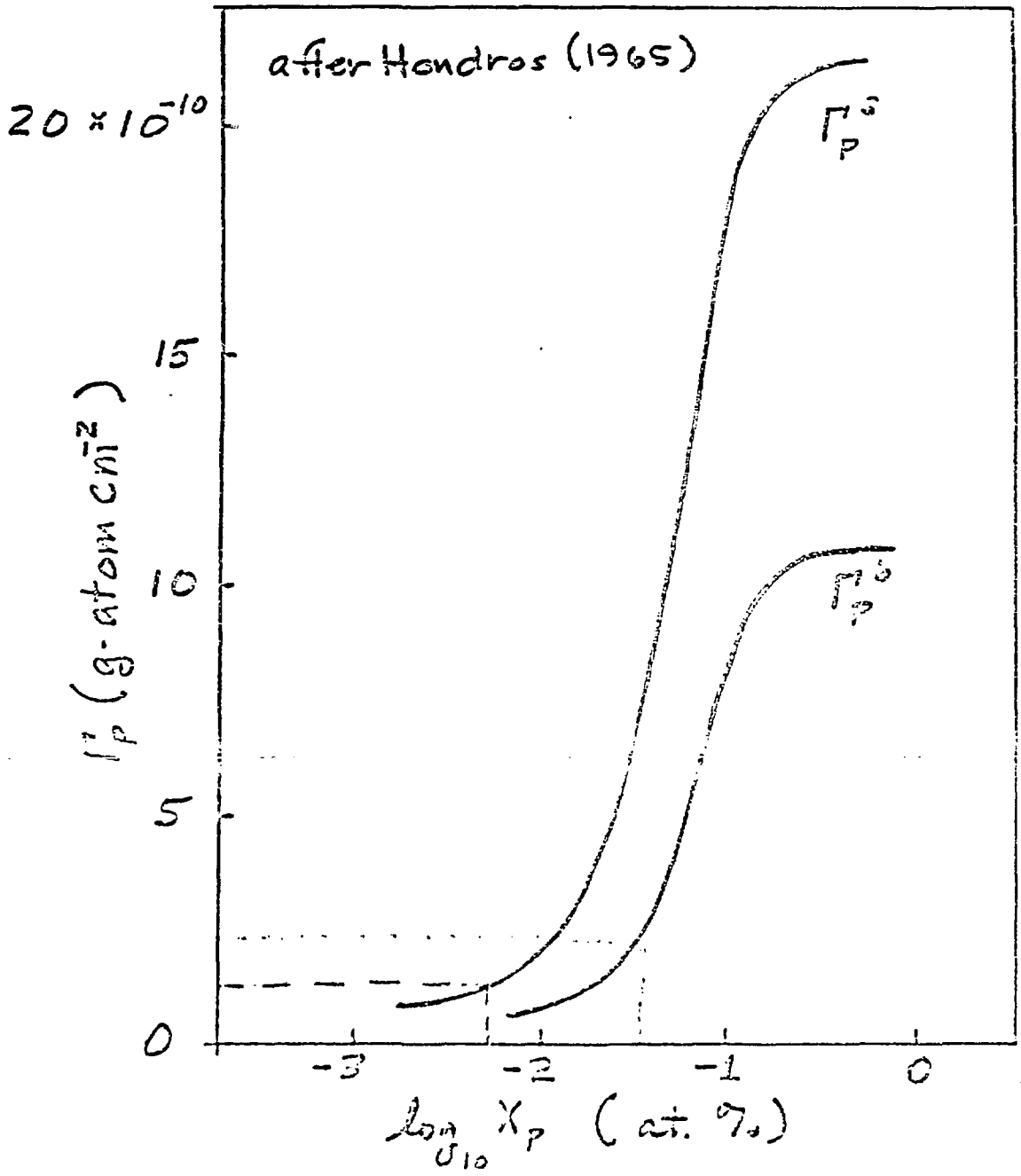

Fig. 6(b) Values of Γ_p^s and Γ_p^b for Fe-P alloys at 1450°C, after Hondros, ref (1).

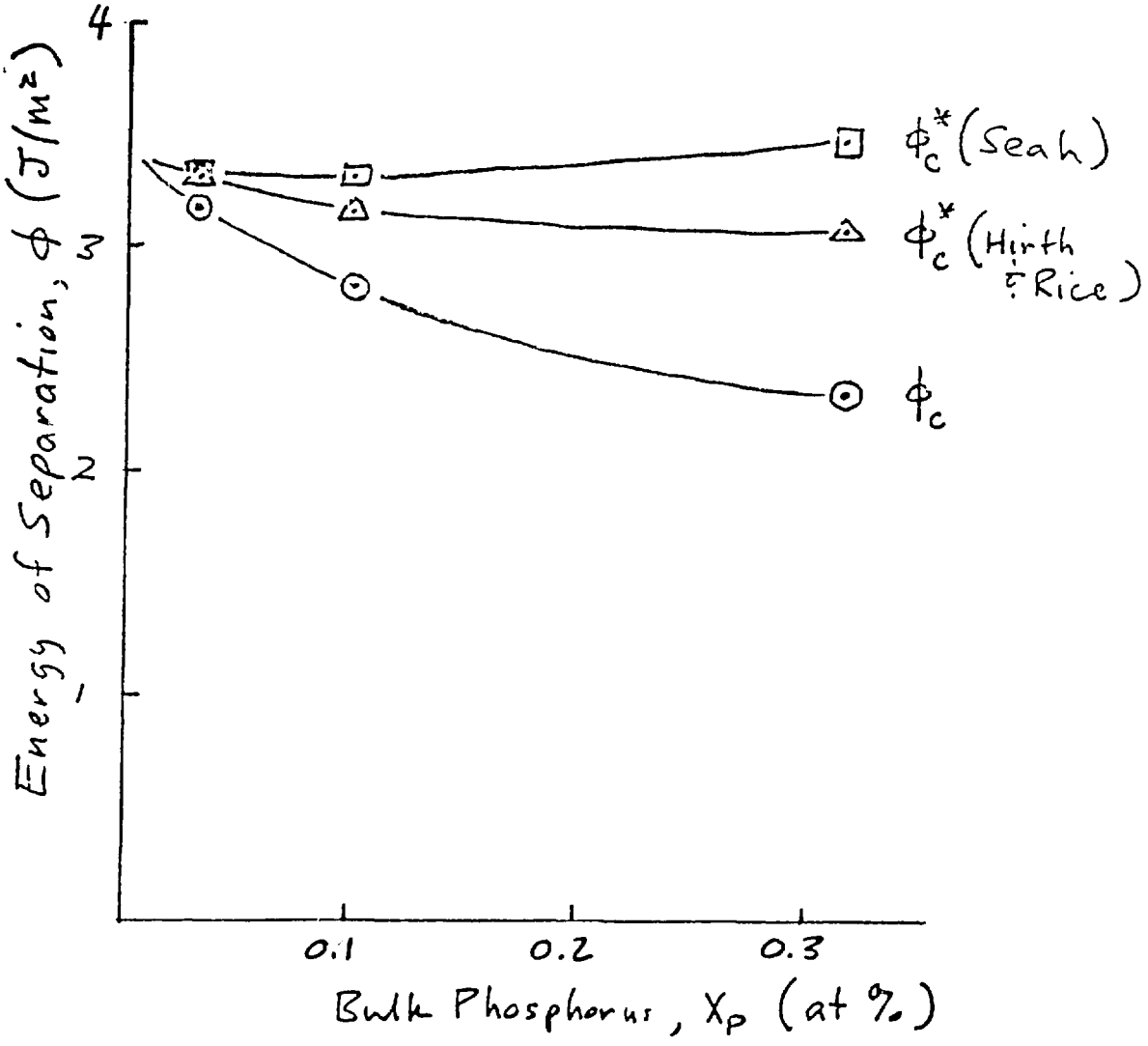

Fig. 7 Plots of the reversable energy of separation, ϕ_c, and irreversable energies of separation, ϕ_c^*, according to Seah, and Hirth and Rice. Calculations made using the experimental data of Hondros for Fe3P alloys at 1450C

Fig. 8

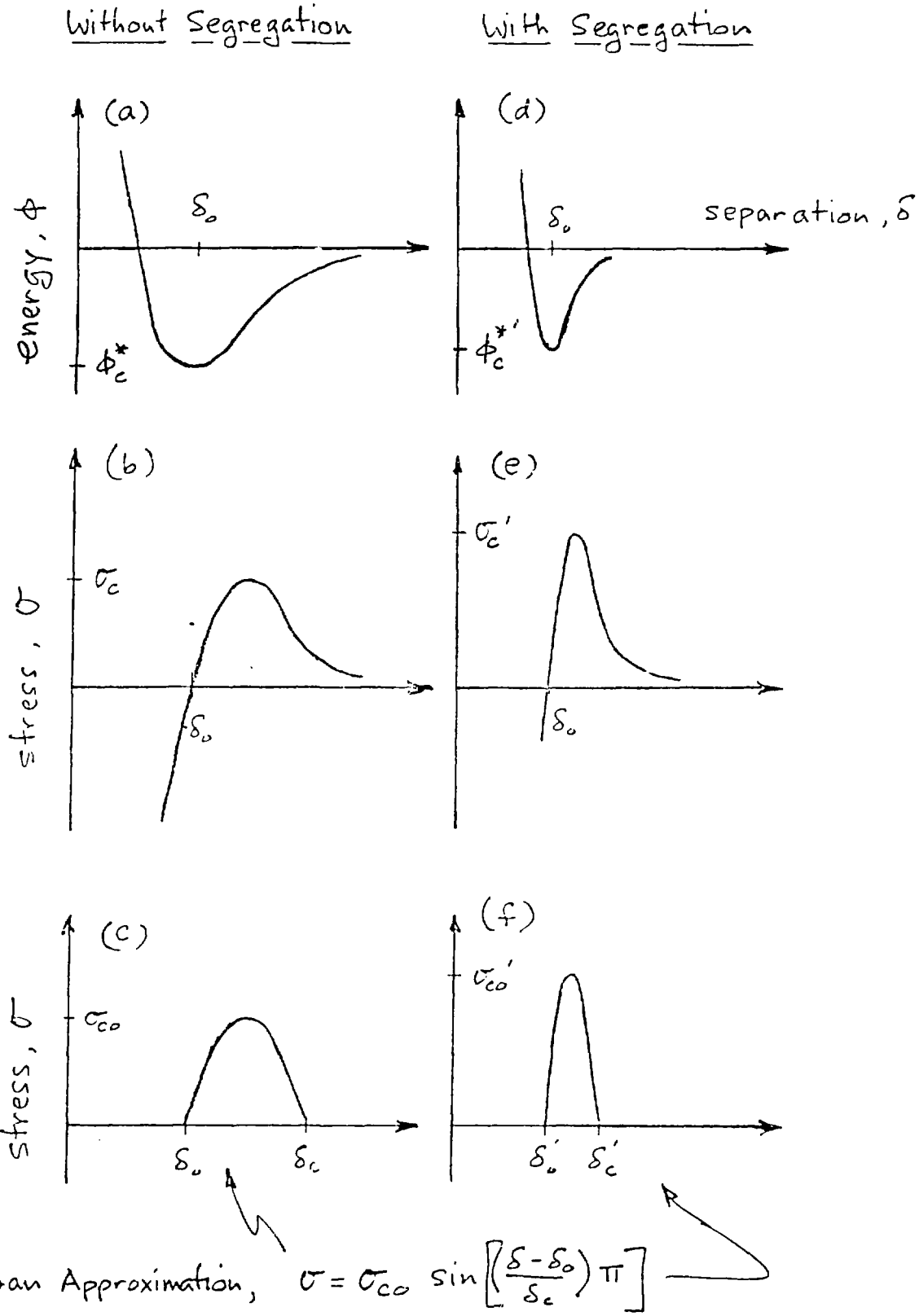
Without Segregation
With Segregation
(a)
(d)
energy, ϕ
δ_o
ϕ_c^*
$\phi_c^{*\prime}$
separation, δ
(b)
(e)
stress, σ
σ_c
σ_c'
δ_o
(c)
(f)
σ_{co}
σ_{co}'
δ_o
δ_c
δ_o'
δ_c'
Orowan Approximation, $\sigma = \sigma_{co} \sin\left[\left(\frac{\delta-\delta_o}{\delta_c}\right)\pi\right]$

Fig. 9

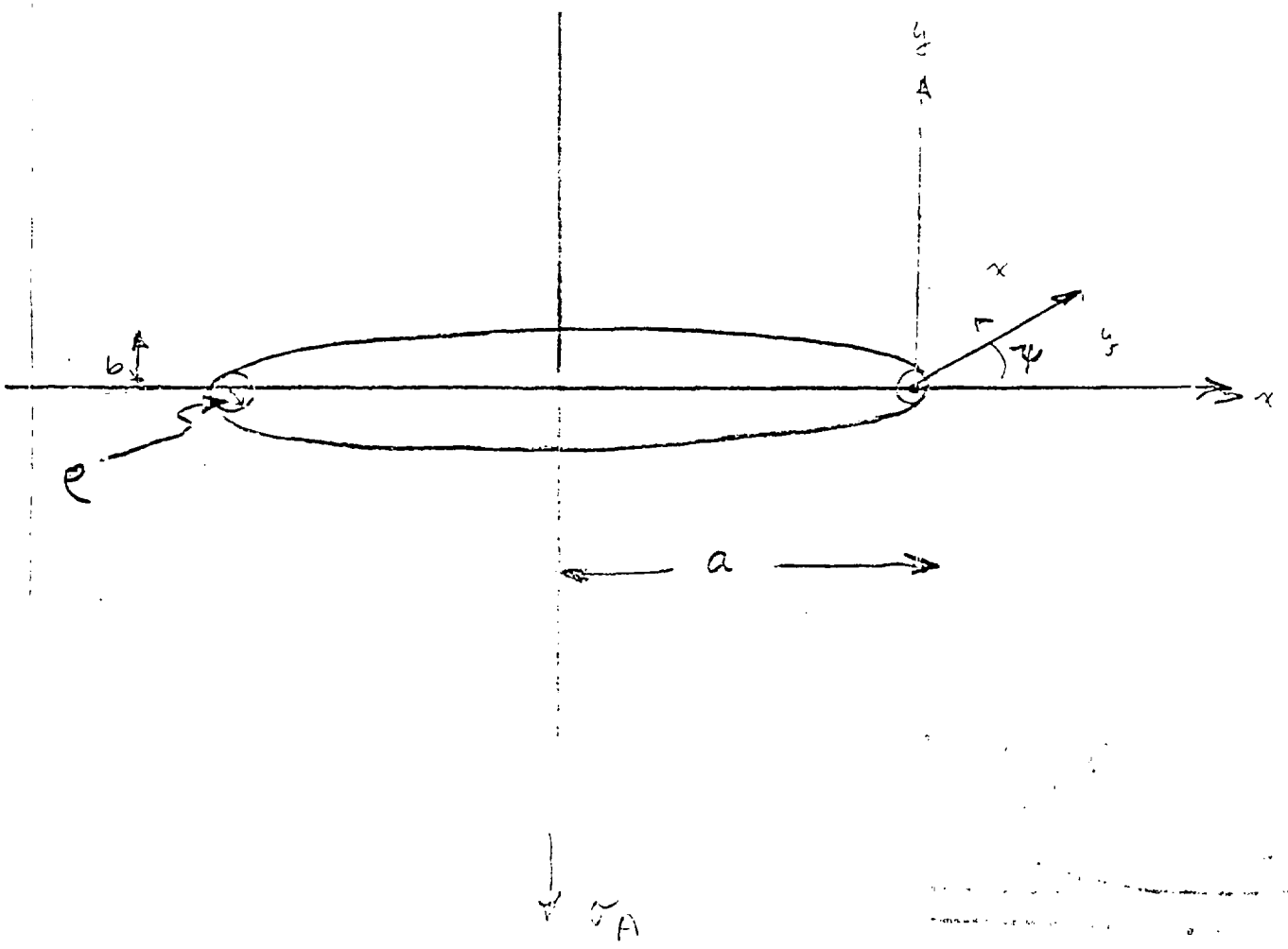

Fig. 10

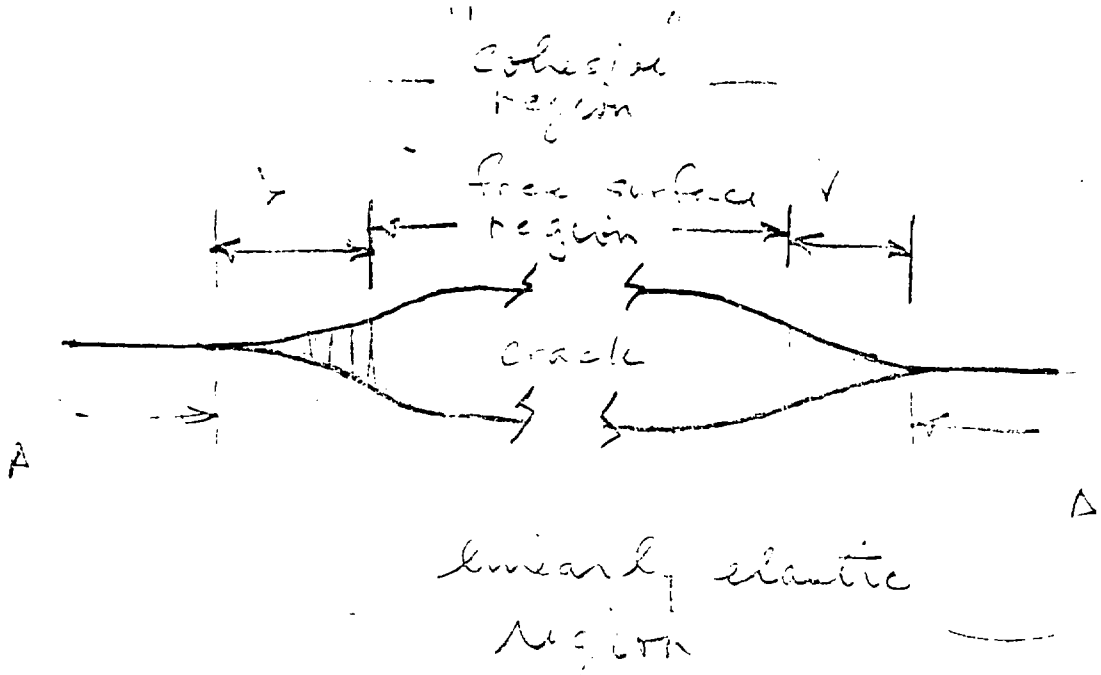

Barenblatt type crack.

Fig. 11

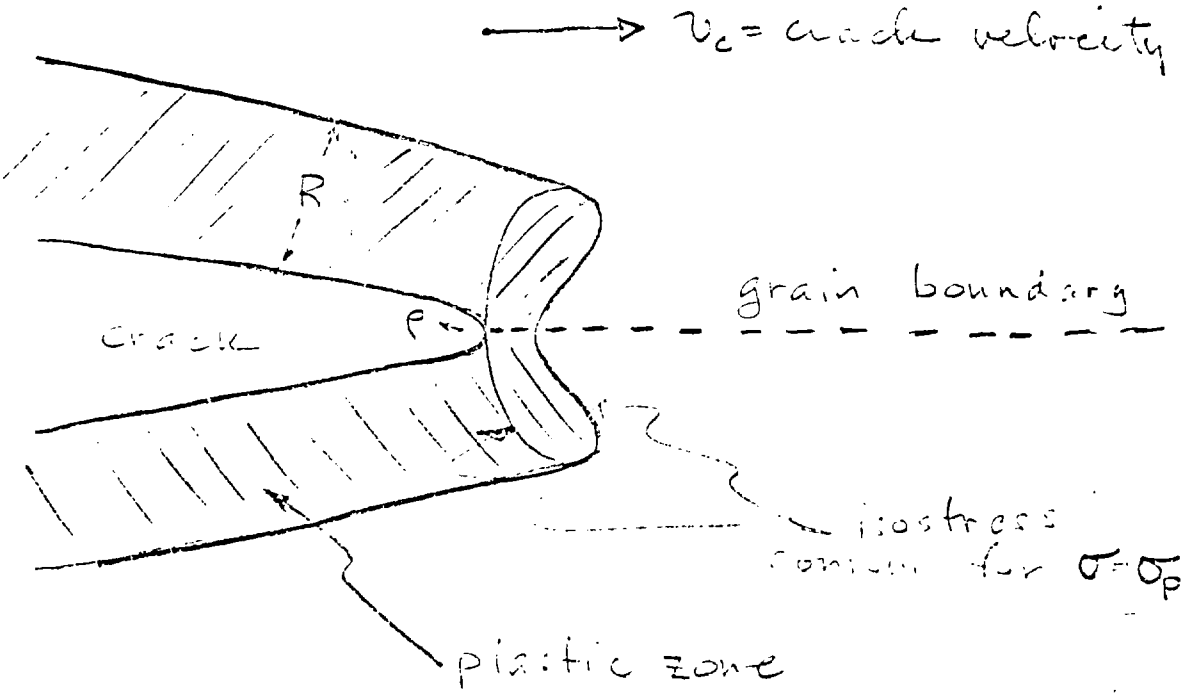
v_c = crack velocity
R
crack
ρ
grain boundary
isostress contour for $\sigma = \sigma_p$
plastic zone

Fig. 12

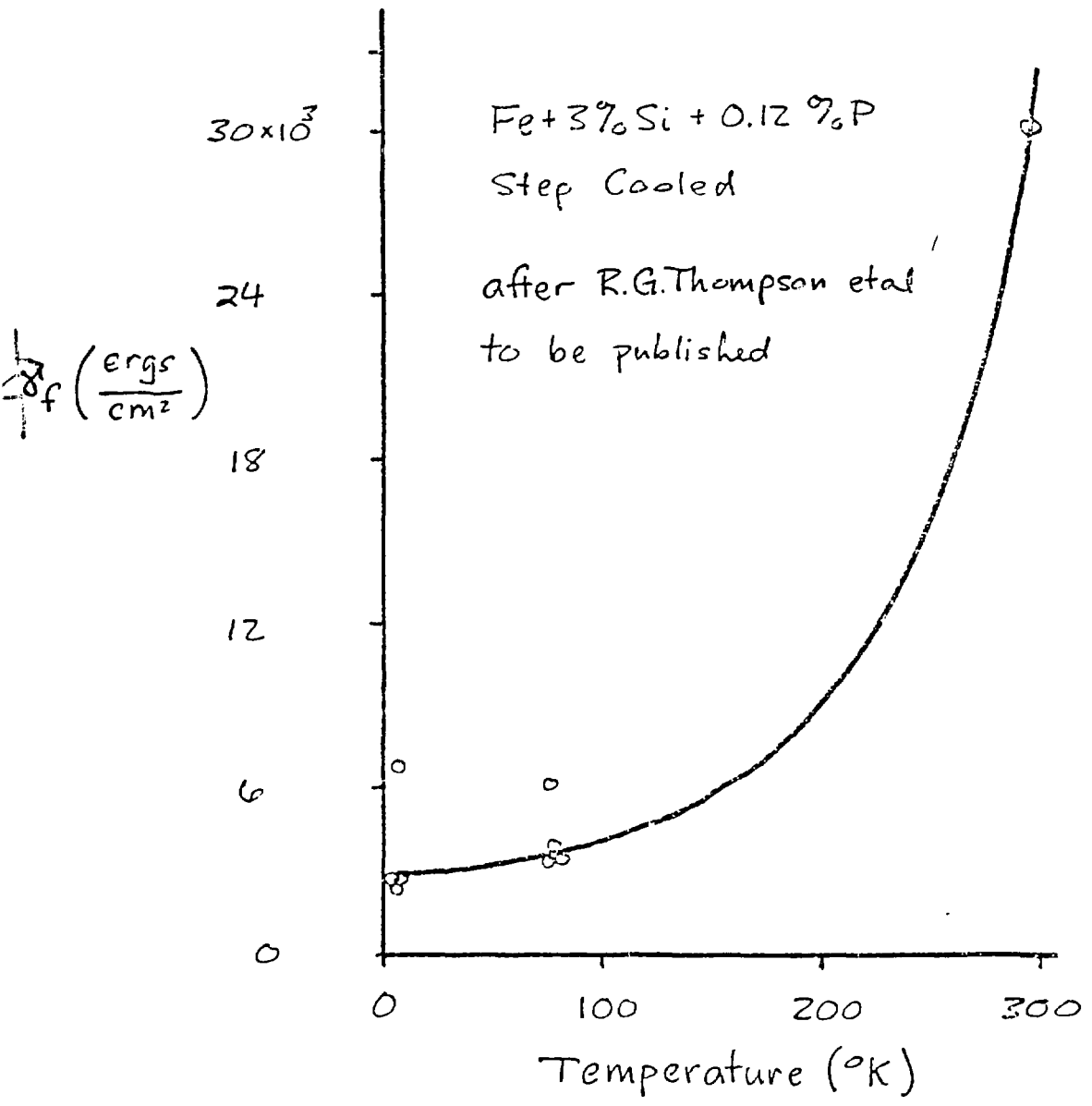
Fe + 3% Si + 0.12 % P
Step Cooled
after R.G. Thompson etal
to be published
$\gamma_f \left(\frac{ergs}{cm^2}\right)$
30 x 10^3
24
18
12
6
0
0
100
200
300
Temperature (°K)

Fig. 13

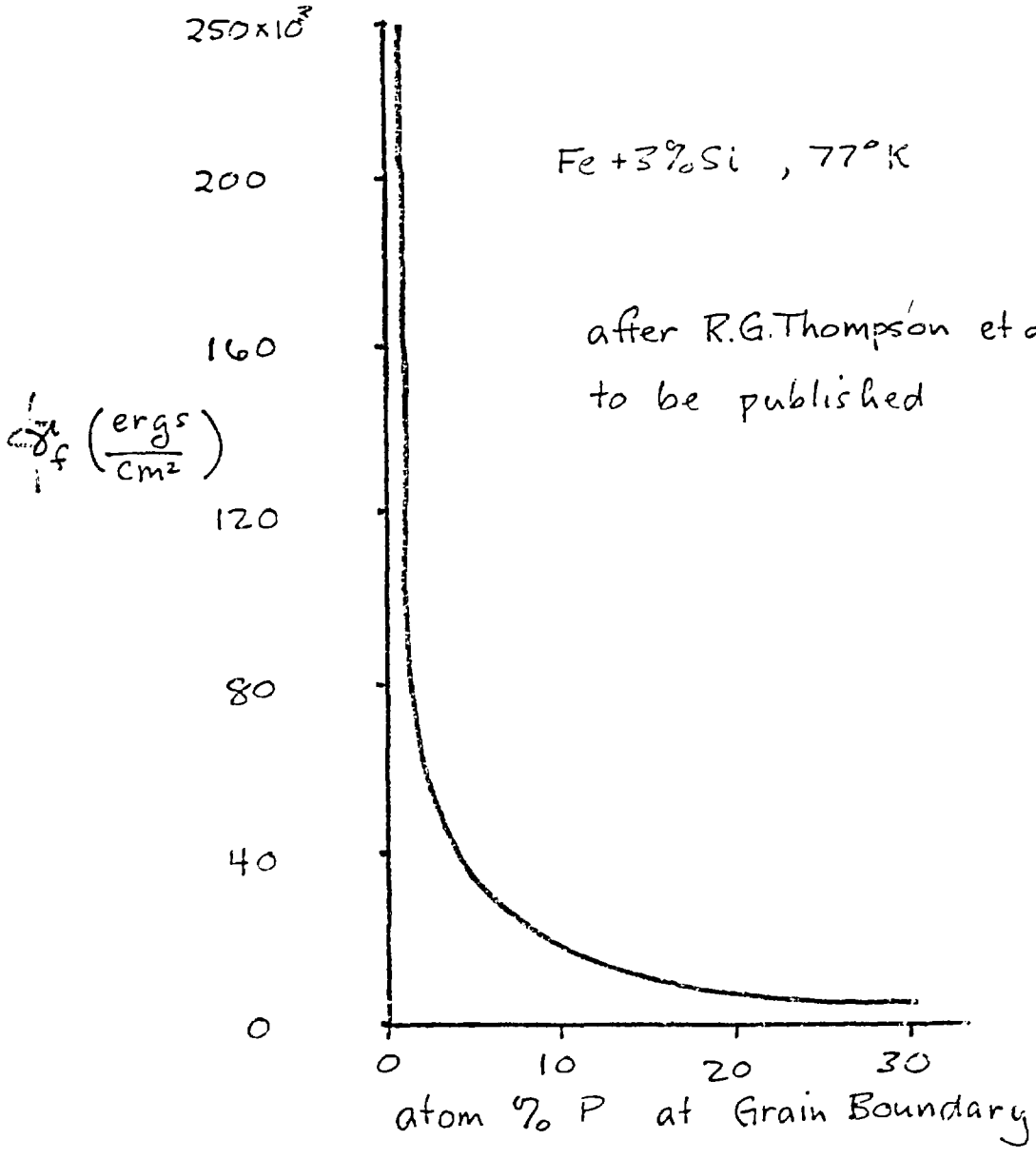
250×10³
200
160
120
80
40
0
σ_f^{γ} $\left(\frac{ergs}{cm^2}\right)$
Fe +3%Si , 77°K
after R.G. Thompson et al
to be published
0
10
20
30
atom % P at Grain Boundary